European Journal of Mechanics / B Fluids 95 (2022) 1–22

Contents lists available at ScienceDirect

European Journal of Mechanics / B Fluids

journal homepage: www.elsevier.com/locate/ejmflu

Multi-phase moving particle semi-implicit method for violent sloshing flows

Xiao Wen, Weiwen Zhao, Decheng Wan *

Computational Marine Hydrodynamics Lab (CMHL), School of Naval Architecture, Ocean and Civil Engineering, Shanghai Jiao Tong University, Shanghai 200240, China

ARTICLE INFO

Article history:
Available online 11 April 2022

Keywords:
MPS
Multi-phase method
Numerical simulation
Violent sloshing flow
Air cushion effect

ABSTRACT

As a meshless technique, the moving particle semi-implicit (MPS) method has extensive applications in numerical studies on violent sloshing flows. However, most prevalent research in the area is based on the single-phase MPS method, which ignores the existence of the air phase. This study aims to illustrate the necessity of multi-phase simulations for representing violently sloshing liquid through a comparative analysis between single-phase and multi-phase MPS methods, and to better figure out the air effect in the violent sloshing flows The MMPS (multi-phase MPS) method is firstly developed by introducing various multi-phase models into the single-phase IMPS (improved MPS) method, and then verified through simulations of two classical examples: the static multi-fluid system and the Rayleigh–Taylor instability. Subsequently, both the MMPS and the IMPS methods are applied to simulate liquid sloshing with increasing intensities, and their numerical results are compared with each other and with experimental data. The comparisons show that as the intensity of sloshing increases, the effect of the air cushion become non-negligible and the accuracy of the single-phase simulation significantly decreases, whereas the simulation results obtained by the MMPS method agree well with the experimental results in all cases. In particular, the MMPS method fully considers the air cavity formed in case of a violent wave breaking as well as its influence on waves of the sloshing liquid, and rectifies the overestimation of impact pressures in single-phase simulations.

1. Introduction

For cargo ships that carry liquids in turbulent waters, the violent sloshing of the liquid can be induced by the movement of the ship such that it forcefully strikes the walls of its container. Moreover, the resonance phenomenon may occur in case of large tanks filled with liquid, causing the slamming force to become sufficiently large for the liquid to break through the tank and compromise the safety of the ship [1–6]. Therefore, it is important to study the mechanism of violently sloshing liquid in a tank to guide the design of cargo ships used to transport it. Computational Fluid Dynamics (CFD) has been an effective approach for studying sloshing flows in recent decades [7–11]. However, when sloshing flows become violent, the strong impact and complex deformations of the phase interface pose daunting challenges to the use of CFD methods to model such phenomena [12–14].

In recent years, the meshless methods, such as the moving particle semi-implicit (MPS)[15–17] and the smoothed particle hydrodynamics (SPH) [18,19], have been widely applied to numerical studies on violent flows and prove to be an effective CFD tool [20–26]. The calculational domain in the MPS and SPH methods is represented by a set of particles in space with distinct physical properties, allowed motions following Lagrangian equations. The particle distribution can be used to obtain the interface between particles of different phases without the need for additional interface-capturing algorithms. Therefore, compared with mesh-based methods, the meshless method is more suitable for representing sloshing flows with strong and nonlinear deformations of the free surface. For example, Debadatta and Kishore [27] performed MPS simulations of the violently sloshing liquid in a container undergoing horizontal sinusoidal motion, in which the dynamic parameters required for optimization design, including the amplitude of the wave, impact pressure, base shear, and overturning moment, were accurately calculated. Hwang et al. [28] combined the MPS method with fluid structure analysis to simulate sloshing flows with elastic baffles, and carefully validated the effect of the baffles in suppressing the development of sloshing flows. Zhang and Wan [29] presented a comparative study between the MPS and level set simulations of the violently sloshing liquid, and the results showed that the peak pressures, wave breakings, and liquid splashing captured by the MPS method were more consistent with experimental data.

* Corresponding author.
E-mail address: dcwan@sjtu.edu.cn (D. Wan).
URL: https://dcwan.sjtu.edu.cn/ (D. Wan).

https://doi.org/10.1016/j.euromechflu.2022.04.002
0997-7546/

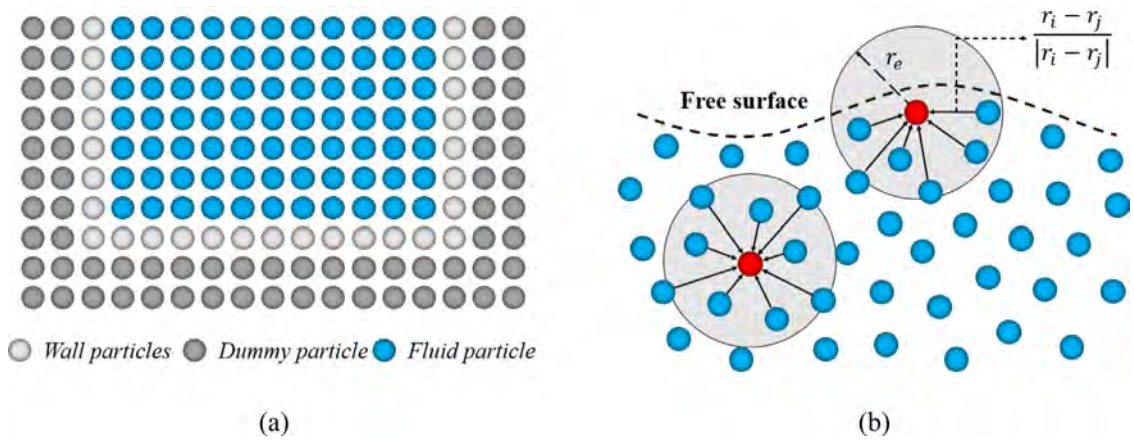

Fig. 1. Schematic of boundary conditions in the MPS method. (a) Wall boundary condition (b) free surface boundary condition.

However, most MPS simulations of violently sloshing liquids are based on the single-phase MPS method, [30–35] which requires the sloshing flows to be simplified as a single-phase model in which the region of air is assumed to be an empty area and the effect of the air phase is ignored. With this simplification, the single-phase MPS method becomes capable to simulate violently sloshing liquids, and, in some cases, yields good agreement with the results of experiments. However, the accuracy of single-phase MPS simulations decreases with the increase in the intensity of sloshing. As has been observed in experiments, [36–40] a massive amount of air is trapped by the overturning and breaking of waves, and has a significant influence on the shape of the sloshing waves that cannot be considered by the single-phase MPS method. Moreover, the air may be trapped between the sloshing waves and the walls of the tank containing the liquid during wave impact, acting as an "air cushion" that affects the accuracy of prediction of the impact pressure [41,42].

Several multi-phase MPS methods have been developed and applied in recent years to simulate a violently sloshing liquid. Shimizu et al. [43] and Meng et al. [44] developed and used multi-phase MPS methods to simulate sloshing flow with a high filling rate, corresponding to an experiment by Koh et al. [45] A good agreement between snapshots of the MPS and the experimental photographs was achieved, and the impact pressures were accurately predicted. However, the sloshing flow studied by them was not sufficiently violent for the overturning and breaking of waves, because of which the deformation in the phase interface was not complicated. Khayyer and Gotoh [46] used the multi-phase MPS method with a consistent pressure gradient that obeyed the Taylor series to reproduce the sloshing experiment performed by Rognebakke et al. [47] The phenomenon of air entrapment due to the impact of sloshing waves on the roof of the tank was successfully captured and a stable pressure field was obtained.

The above studies constitute almost all work on multi-phase MPS simulations of sloshing flows, but do not well consider the problems of sloshing flows with overturning and breaking waves. This study aims to illustrate the necessity of multi-phase simulations for representing violently sloshing liquid through a comparative analysis between single-phase and multi-phase MPS methods, and to better figure out the air effect in the violent sloshing flows. A multi-phase MPS method that is highly stable and accurate is first developed and verified through two classical examples: the static multi-fluid system and the Rayleigh–Taylor instability. Both single-phase and multi-phase MPS methods are then applied to simulate three different problems of sloshing flows with increasing intensities. The results for the different cases are finally used to analyze the effect of the air phase and establish the superiority of the multi-phase MPS method.

2. IMPS method

The IMPS (improved MPS) method, [49–52] proposed and widely validated by the Computational Marine Hydrodynamics Lab (CMHL), is employed for the single-phase simulations in this paper. In this method, four enhanced schemes are used to suppress pressure oscillations of the original MPS method: (1) the gradient model of momentum conservation, (2) the kernel function without singularity, (3) the Pressure Poisson Equation (PPE) with a mixed source term, and (4) the highly precise approach for free surface detection. In this section, the IMPS method would be introduced in detail.

2.1. Governing equations

The governing equations of MPS method consist of equations for the conservation of mass and momentum [16] with the following Lagrangian forms:

$$\frac{D\rho}{Dt} = -\rho(\nabla \cdot \boldsymbol{u}) \tag{1}$$

$$\rho\frac{Du}{Dt} = -\nabla P + \boldsymbol{F}^V + \boldsymbol{F}^B + \boldsymbol{F}^S \tag{2}$$

where ρ, $\boldsymbol{u}$, and P represent the density, velocity, and pressure of the particles, respectively, $\boldsymbol{F}^V$, $\boldsymbol{F}^B$, and $\boldsymbol{F}^S$ denote the viscous force, body force, and surface tension forces, respectively. Note that, the surface tension force $\boldsymbol{F}^S$ is usually ignored in the single-phase MPS simulation.

2.2. Kernel function

There are various forms of interactions between neighboring particles in the MPS method, and the kernel function is used as a weight function to measure the strength of these interactions. For the IMPS method, the improved kernel function proposed by Zhang and Wan [52] is adopted:

$$W(r_{ij},\ r_e) = \begin{cases} \frac{r_e}{0.85r_{ij}+0.15r_e} - 1 & (0 \le r < r_e) \\ 0 & (r_e \le r) \end{cases} \tag{3}$$

where r_{ij} and r_e represent the distance between particles and the largest radius of particle interaction, respectively. The default size [16] of r_e is $2.1dp$ for the gradient and divergence models, and $4.1dp$ for the Laplace model, where dp represents the initial particles distance. As the distance between particles decreases, the value of kernel function increases, resulting in stronger particle interactions, and vice versa. When the distance between a pair of particles is larger than a certain threshold, the kernel function

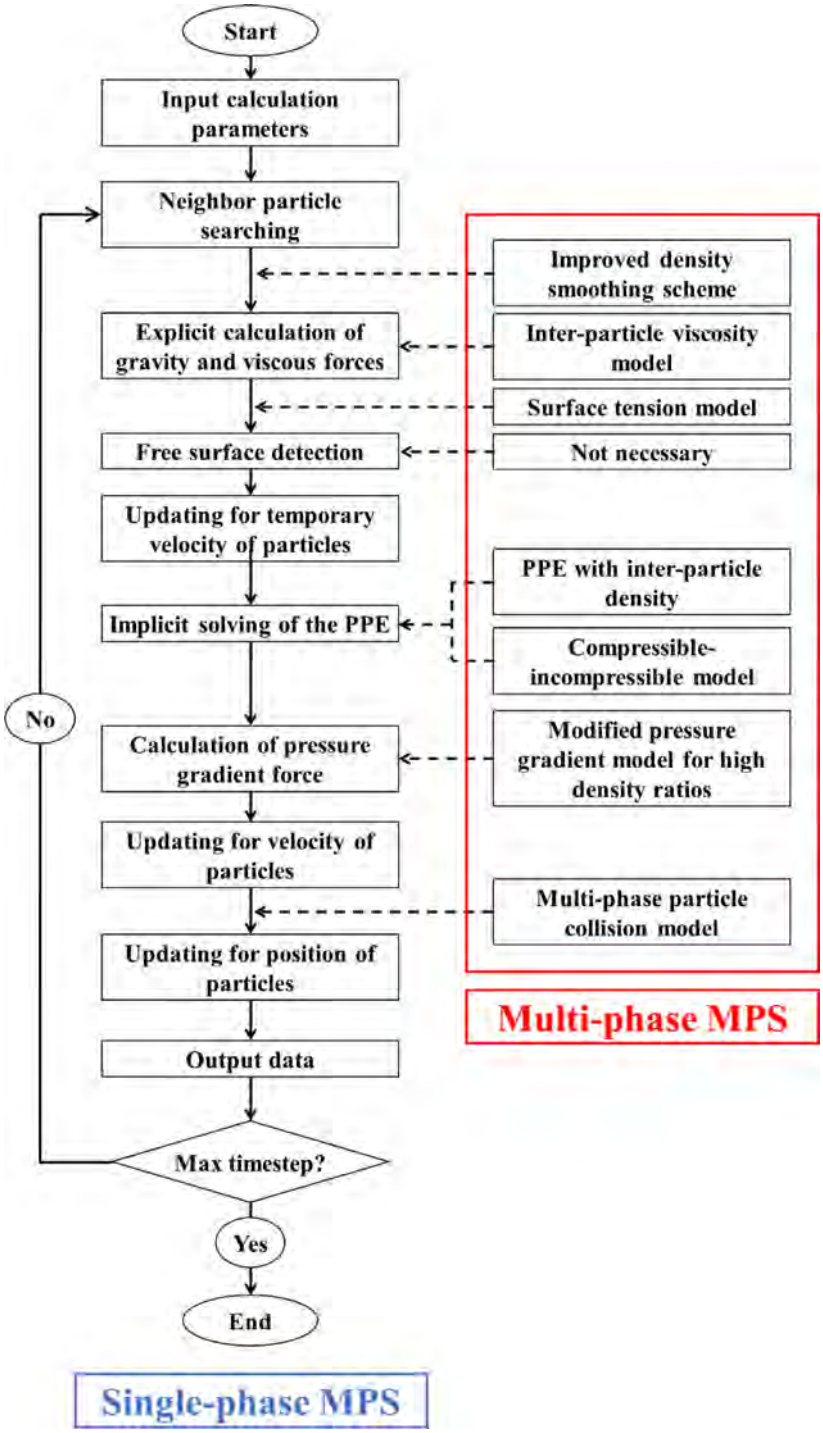

Fig. 2. Flowchart of single-phase and multi-phase MPS methods.

becomes zero and no interaction occurs. The improved kernel function obtains a finite value when the particle distance is zero. Thus, the problem of singularity of the original kernel function [16] can be well avoided.

2.3. Particle interaction models

Particle interaction models [16] are employed to discretize the differential operators in the governing equations, including the gradient model, divergence model, and Laplacian model:

$$\langle \nabla \phi \rangle_i = \frac{D}{n^0} \sum_{j \neq i} \frac{\phi_j - \phi_i}{|\boldsymbol{r}_j - \boldsymbol{r}_i|^2} (\boldsymbol{r}_j - \boldsymbol{r}_i) W(r_{ij}, r_e) \tag{4}$$

$$\langle \nabla \cdot \Phi \rangle_i = \frac{D}{n^0} \sum_{j \neq i} \frac{(\Phi_j - \Phi_i)}{|r_j - r_i|^2} \cdot (r_j - r_i) W(r_{ij}, r_e) \tag{5}$$

$$\langle \nabla^2 \phi \rangle_i = \frac{2D}{n^0 \lambda} \sum_{j \neq i} (\phi_j - \phi_i) W(r_{ij}, r_e) \tag{6}$$

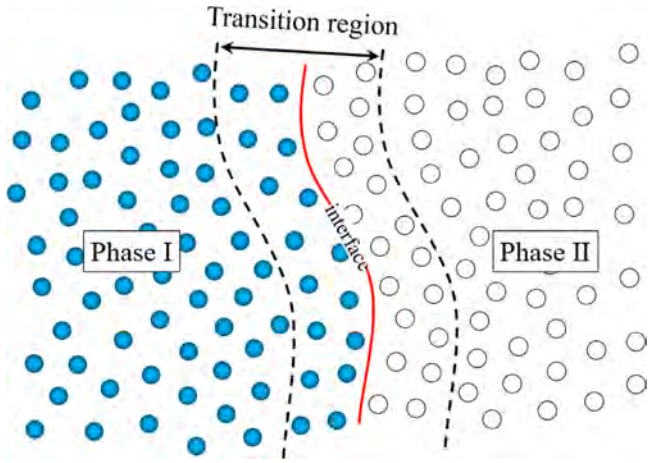

Fig. 3. Illustration of transition region defined in the MMPS method.

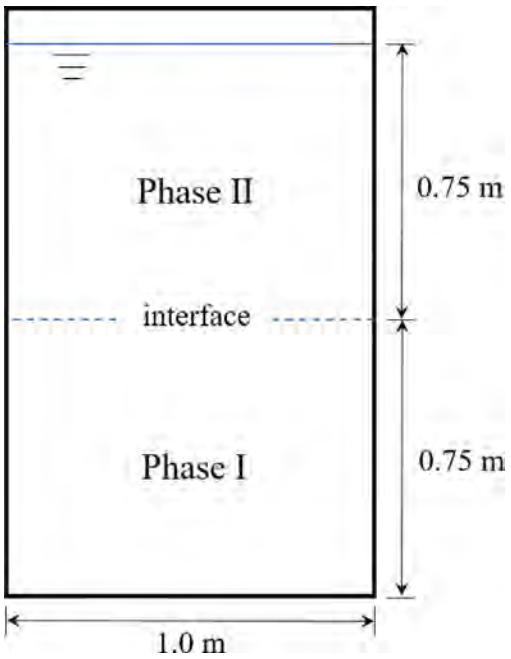

Fig. 4. Initial setup of the static multi-fluid system.

where ϕ is an arbitrary scalar function, θ is an arbitrary vector, D is the number of spatial dimensions, n^0 is the particle number density in the initial arrangement, calculated as

$$\langle n\rangle_i = \sum_{j\neq i} W(r_{ij},\ r_e) \tag{7}$$

and λ is a parameter to keep the increase in variance equal to that in the analytical solution. It can be calculated as:

$$\lambda = \frac{\sum_{j\neq i} W(r_{ij},\ r_e)|r_j - r_i|^2}{\sum_{j\neq i} W(r_{ij},\ r_e)} \tag{8}$$

2.4. Pressure gradient model

When the gradient model given in Eq. (4) is used to calculate the pressure gradient force, the conservation of linear and angular moments cannot be fully satisfied, and this may cause significant tensile instability. To overcome this, the IMPS method adopted the following conservative form proposed by Tanaka and Masunaga [53]:

$$\langle \nabla P\rangle_i = \frac{D}{n^0}\sum_{j\neq i}(P_j + P_i)\frac{(\boldsymbol{r}_j - \boldsymbol{r}_i)}{|\boldsymbol{r}_j - \boldsymbol{r}_i|^2} W(r_{ij},\ r_e) \tag{9}$$

With the above model, the pure repulsive force between particles can be guaranteed, thus the problem of tensile instability is solved.

2.5. Semi-implicit algorithm

To maintain the incompressibility of fluid, a semi-implicit algorithm [16] is used in the MPS method whereby each timestep is divided into a (first) prediction step and a (second) correction step. This is also the main difference between the MPS method and the original SPH method. In recent years, the semi-implicit algorithm is also introduced into the SPH method, through which the ISPH (Incompressible SPH) method [54] is further proposed.

In the prediction step, the temporal velocity field is explicitly updated according to the viscous force, gravitational force, and surface tension force. Then in the correction step, the PPE is solved to obtain the pressure field, through which the velocities and locations of the particles are updated to the next time step. In the IMPS method, the PPE with a mixed source term, proposed by Tanaka and Masunaga [53] and rewritten by Lee et al. [55], is used:

$$\langle \nabla^2 P^{k+1}\rangle_i = (1-\gamma)\frac{\rho}{\Delta t}\nabla\cdot\boldsymbol{u}_i^* - \gamma\frac{\rho}{\Delta t^2}\frac{\langle n^k\rangle_i - n^0}{n^0} \tag{10}$$

where γ is a blending parameter less than 1, $\boldsymbol{u}_i^*$ is the temporal velocity, and $< n^k >_i$ is the particle number density at the kth time step. According to the numerical tests by Lee et al. [55], the pressure oscillations can be well suppressed at $\gamma = 0.01$, which is followed in the present study. As Tanaka and Masunaga [53] have noted, the mixed source term is in fact a combination of the divergence free velocity condition and the constant particle number density condition, which is favorable for the numerical stability.

2.6. Boundary conditions

The wall boundary condition in the MPS method can be regarded as a kind of impenetrable condition, and is imposed by the arrangement of the wall and dummy particles, as shown in Fig. 1(a). For the simulations of liquid sloshing, the velocity of wall particles is directly given according to the tank motion. A single layer of wall particles in contact with the fluid domain participates in the solution of the PPE together with the fluid particles, whereas the pressures of dummy particles are obtained through an interpolation based on the pressures of neighboring fluid and wall particles. When the fluid particles get too close to the wall, the pressure of wall particles increases rapidly, and a pressure gradient force opposite to the wall is exerted on the fluid particles. Nonphysical penetrations can thus be prevented.

With regard to the boundary of the free surface, a Dirichlet boundary condition of zero pressure is imposed for all free surface particles. To accurately identify the free surface particles, the IMPS method adopted a highly precise approach [56] in which a vector is defined to quantitatively assess the asymmetry of particle distribution:

$$\boldsymbol{A}_i = \frac{D}{n^0}\sum_{j\neq i}\frac{(\boldsymbol{r}_i - \boldsymbol{r}_j)}{|\boldsymbol{r}_i - \boldsymbol{r}_j|} W(r_{ij}, r_e) \tag{11}$$

In case of free surface particles, all neighboring particles are located on the liquid side, as shown in Fig. 1(b). Therefore, the

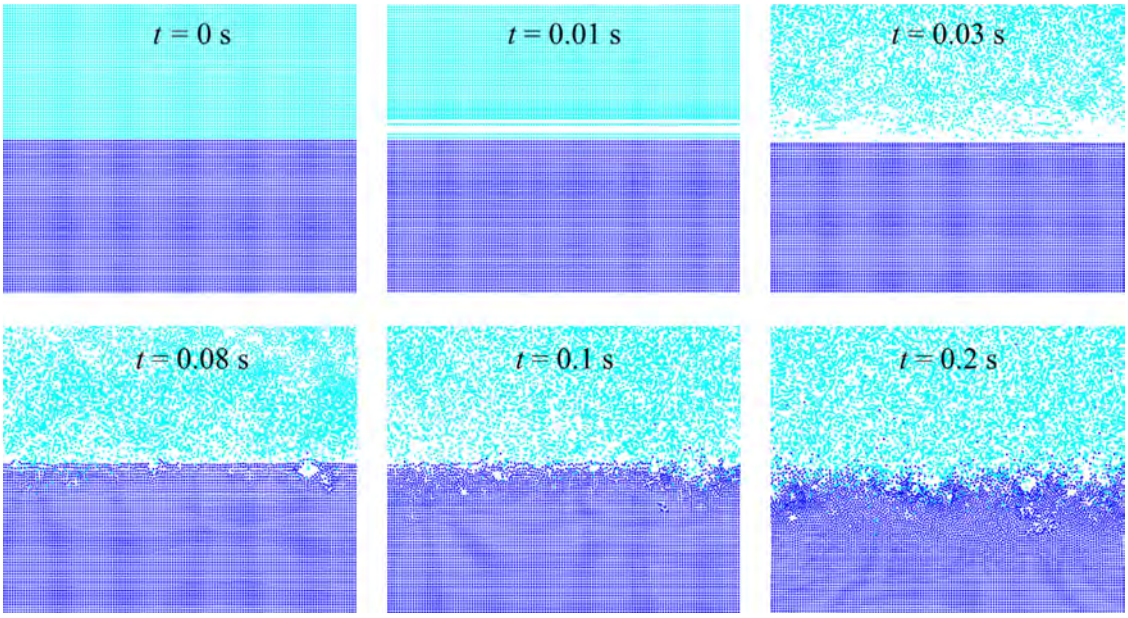

Fig. 5. Snapshots of local particle distribution near the phase interface as simulated by the IMPS method.

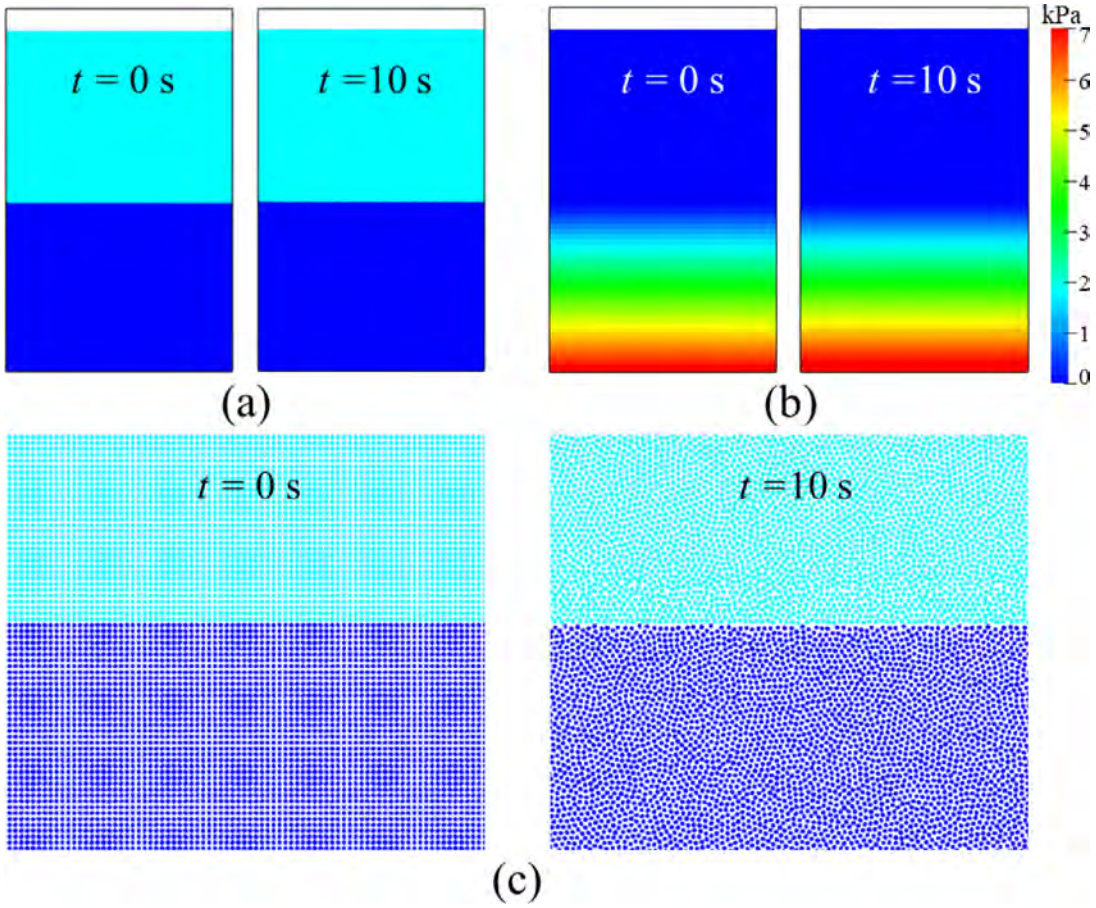

Fig. 6. Results of numerical simulations of the static multi-fluid system obtained by the MMPS method. (a) Phase field. (b) Pressure field. (c) Local particle distribution on the phase interface.

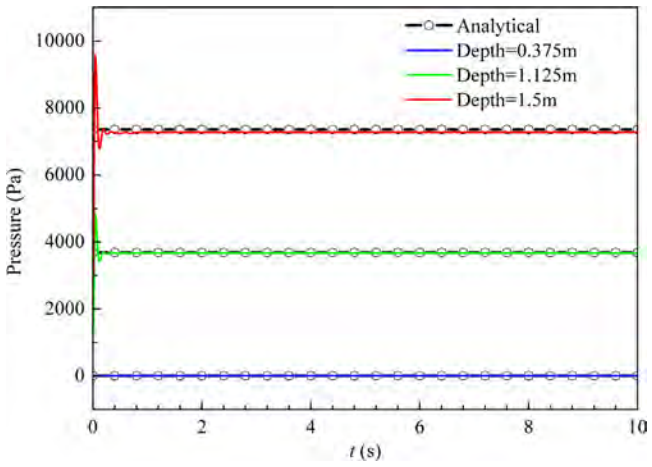

Fig. 7. Comparison of hydrostatic pressures between the numerical results and the analytical solutions at three depths.

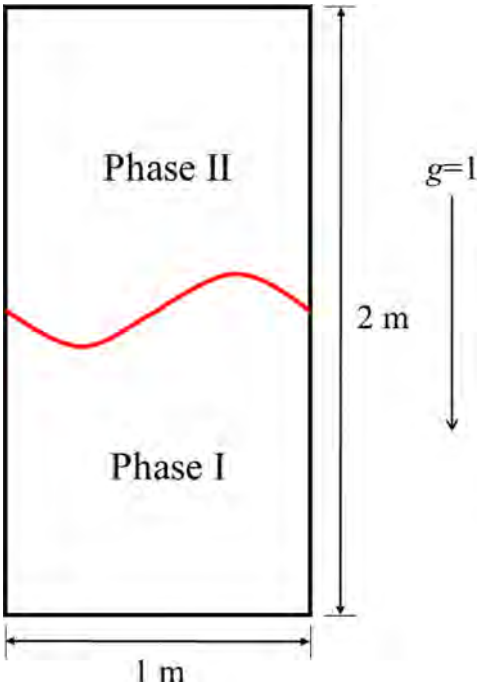

Fig. 8. Schematic of the RTI problem with a single sinusoidal disturbance.

high asymmetry and low particle number density are considered as the main two criteria in this approach, and the particles satisfying the following conditions are judged as free surface particles:

$$\begin{gathered} \langle n\rangle_i < \beta_1 n^0 \\ \text{or} \\ \langle n\rangle_i > \beta_1 n^0 \ \text{ and } \langle n\rangle_i \langle \beta_2 n^0 \ \text{ and } |\boldsymbol{A}|_i \rangle \alpha |\boldsymbol{A}|^0 \end{gathered} \tag{12}$$

where $\alpha = 0.9$, $\beta_1 = 0.8$, $\beta_2 = 0.97$, and $|\boldsymbol{A}|^0$ represents the initial value of $|\boldsymbol{A}|$ for free surface particles. Note that the above judgment is needless in the multi-phase MPS method, where zero pressure is assigned to the uppermost layer of air particles in the computational domain and the pressures of interface particles are obtained by solving the PPE.

3. MMPS method

The multi-phase simulation in this study is performed with the MMPS method [57] developed by introducing various multi-phase models into the IMPS method, including (1) improved density smoothing scheme, (2) inter-particle viscosity model, (3) PPE with inter-particle density, (4) modified pressure gradient model for high density ratios, (5) continuum surface force (CSF) model, (6) multi-phase particle collision model, and (7) compressible–incompressible coupling model. The multi-phase system is treated as a single-fluid system with multi-density and multi-viscosity fields in the MMPS method. Therefore, the governing equations of different phases possess similar forms and can be computed simultaneously. Fig. 2 shows the flowchart of single-phase and multi-phase MPS methods. The MMPS method can be conveniently implemented by adding the multi-phase models to the calculation process of the single-phase MPS method. In the following parts of this section, the multi-phase models in the MMPS method are presented in detail.

3.1. Improved density smoothing scheme

For sloshing flows, the density ratio of the water and air phases is quite high, and the density field is mathematically discontinuous at the phase interface. To overcome the numerical instability induced by this discontinuity, a transition region is defined in the vicinity of the phase interface, as shown in Fig. 3. Within the transition region, an improved density smoothing scheme is applied, which carries out the spatially weighted average density of particles using the following formula:

$$\langle \rho \rangle_i = \frac{\rho_i W_{\text{self}} + \sum_{j\in I} \rho_j W(r_{ij},\, r_e)}{W_{\text{self}} + \sum_{j\in I} W(r_{ij},\, r_e)} \tag{13}$$

where I includes the target particle i and all its neighboring particles. From the above density smoothing scheme, it can be noted that the width of transition region should be equal to $2r_e$. Considering that the smaller transition region is closer to the physical interface, we adopt $r_e = 2.1dp$ in the density smoothing scheme. W_{self} is a weight function to magnify the influence of the target particle itself, so that the smoothed density field is closer to the real density field. Therefore, compared with the original scheme [58] proposed for problems involving the low density ratio, the improved scheme maintains the sharpness of the variation in density, and some sloshing features associated with the high density ratio can be better captured.

Although the density smoothing scheme induces the mathematical variation of fluid density, it would not affect the incompressibility of fluid. The reason is that the concept of Particle Number Density (PND) [16] is introduced into MPS and acts as the new criterion of fluid incompressibility. As can be seen from the PPE in Eq. (10), the fluid incompressibility is satisfied when the PND remains constant, which is not related to the fluid density, but only decided by the distribution of particles. Hence, the smoothing of fluid density mainly improves the calculated results of pressure field, pressure gradient and particle acceleration.

3.2. Inter-particle viscosity model

There is also a discontinuity of viscosity field existing across the phase interface, which would affect the calculation accuracy of viscous force inside the transition region. To deal with this, the inter-particle viscosity model [58] is employed in the MMPS method. Specifically, when particles belonging to different phases interact with each other, the inter-particle viscosity is defined to substitute the real viscosity in the calculation of viscous force.

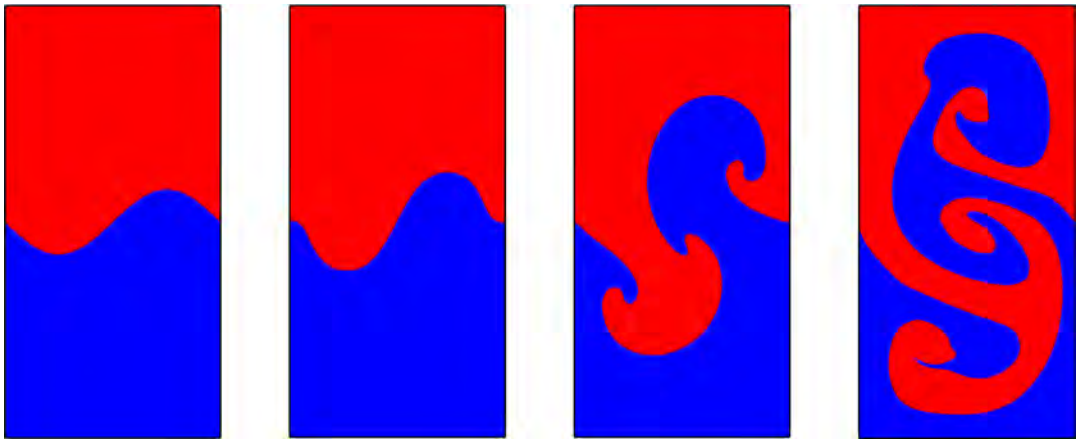

Fig. 9. Evolution of RTI as simulated by the MMPS method ($t = 0$ s, 1 s, 3 s, 5 s).

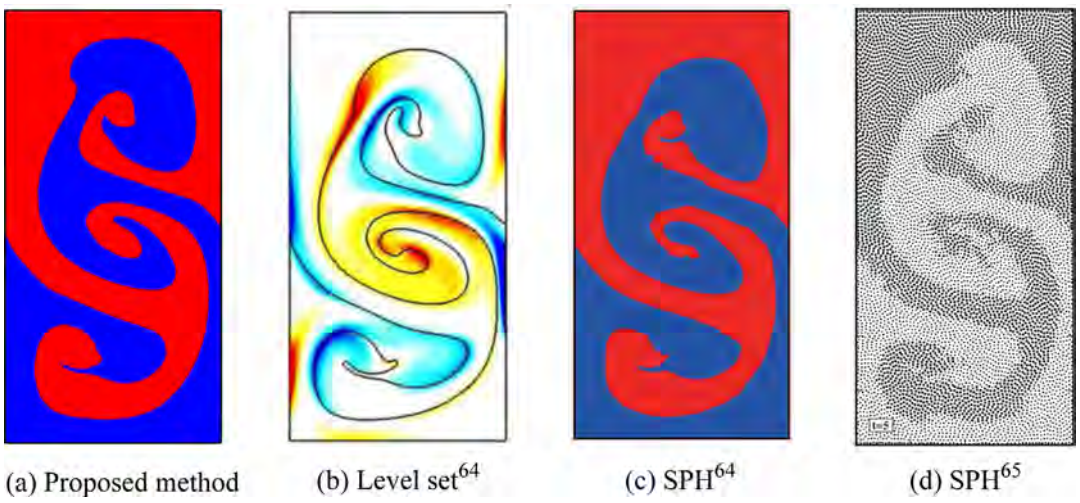

Fig. 10. Comparison of RTI interfaces captured by different numerical methods ($t = 5$ s).

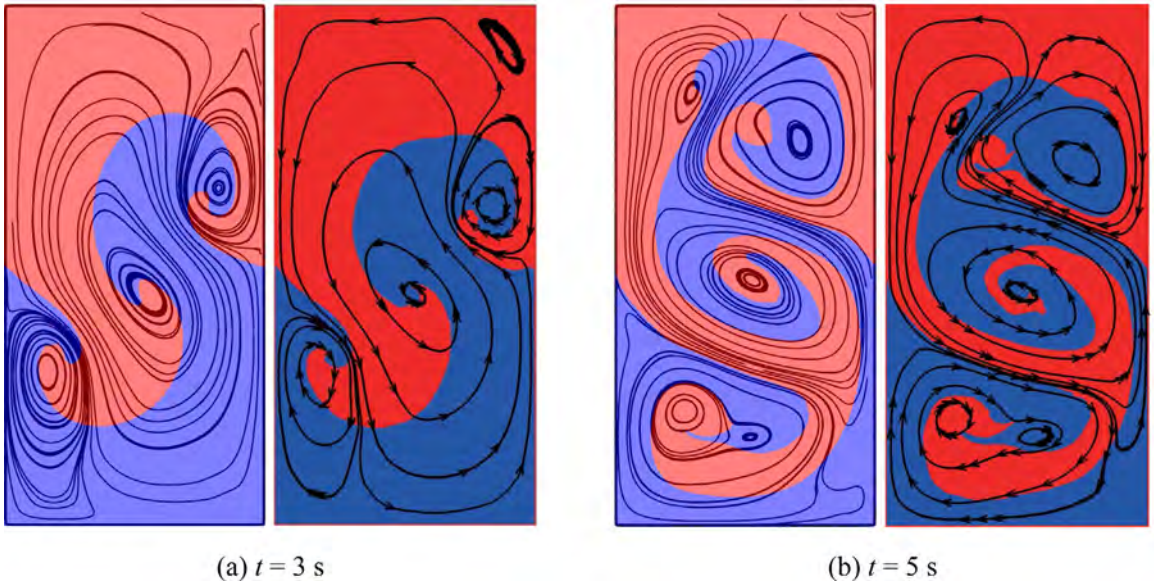

Fig. 11. Comparison of streamline distribution and evolution of vortices in RTI problems between the MMPS (left) and the SPH [48] (right) methods.

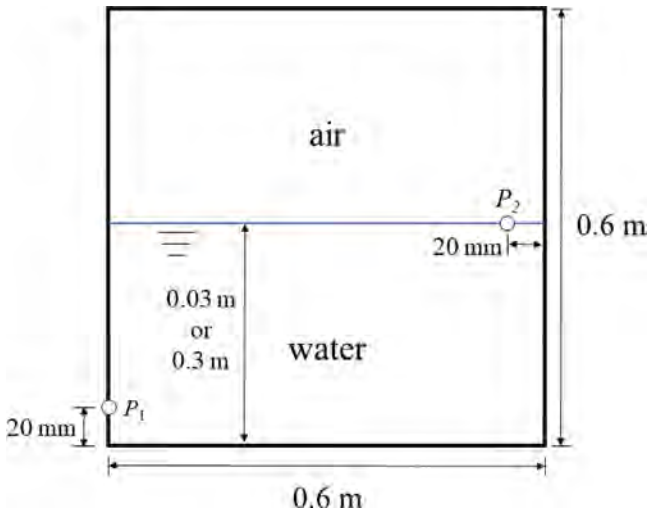

Fig. 12. Numerical model of the sloshing without wave breaking or with mild wave breaking.

The inter-particle viscosity can be obtained by averaging the viscosities of different particle:

$$\mu_{ij} = \left[(\mu_i^\theta + \mu_j^\theta)/2\right]^{1/\theta} \tag{14}$$

where μ_{ij} represents the inter-particle viscosity, μ_i and μ_j represent the dynamic viscosities of particles i and j, respectively, and θ is a parameter determining the averaging method. For $\theta = 1$, the arithmetic mean is used. For $\theta = -1$, the harmonic mean is used. According to the recommendations of Shakibaeinia and Jin, [58] the harmonic mean of the inter-particle viscosity is used in the MMPS method. Thus, the viscosity term has the following form:

$$\begin{aligned} \boldsymbol{F}^V &= \nabla\tau = \nabla(\mu\nabla\cdot\boldsymbol{u}) = \nabla\mu(\nabla\cdot\boldsymbol{u}) + \mu\nabla^2\boldsymbol{u} \approx \mu\nabla^2\boldsymbol{u} \\ &= \frac{2D}{n^0\lambda}\sum_{j\neq i}\frac{2\mu_i\mu_j}{\mu_i+\mu_j}(\boldsymbol{u}_j - \boldsymbol{u}_i)W(r_{ij},\, r_e) \end{aligned} \tag{15}$$

In the above formula, the first term $\nabla\mu(\nabla\cdot\boldsymbol{u})$ is equal to zero for incompressible fluid since the divergence free velocity condition can be satisfied. In addition, for compressible fluid, the order of magnitude this term $\nabla\mu(\nabla\cdot\boldsymbol{u})$ is much smaller than that of the second term $\mu\nabla^2 u$ when the value of compressibility is limited. Therefore, this term is neglected in calculations of this study for the sake of simplicity.

3.3. PPE with inter-particle density

In the transition region, the pressure field undergoes significant changes owing to the rapid variation of the density field. Thus, the large pressure gradient may be generated and causes the particles to unphysically move, especially for the lighter particles. To maintain the smoothness of the pressure field, the PPE with inter-particle density [61] is adopted in the MMPS method. Using it, the left-hand side of the PPE can be discretized as

$$\langle\frac{1}{\rho_{ij}}\nabla^2 P^{k+1}\rangle_i = \frac{2D}{n^0\lambda}\sum_{j\neq i}\frac{1}{\rho_{ij}}(P_j^{k+1} - P_i^{k+1})W(r_{ij},\, r_e) \tag{16}$$

where ρ_{ij} is the inter-particle density. Its definition is similar to that of μ_{ij} in Eq. (14), but the arithmetic mean is used here according to the numerical tests by Duan et al. [61], written as:

$$\rho_{ij} = \frac{\rho_i + \rho_j}{2} \tag{17}$$

3.4. Modified pressure gradient model for high density ratios

When calculated with the gradient model of the single-phase MPS method, such as Eq. (4) or Eq. (9), the pressure gradient forces between a pair of interacting particles have the same value. However, the consistency of forces causes a significant discrepancy in the accelerations of particles with different densities. Specifically, owing to the high density ratio, the acceleration of the lighter particles may be significantly overestimated compared with that of the heavier particles, resulting in numerical instability. In the MMPS method, the modified pressure gradient model [61] for high density ratios is used to obtain a continuous and stable acceleration field:

$$\begin{aligned} \langle\frac{1}{\rho_{ij}}\nabla P\rangle_i = &\frac{D}{n^0}\sum_{j\neq i}\frac{2(P_j - P_i)}{\rho_i+\rho_j}\frac{(\boldsymbol{r}_j - \boldsymbol{r}_i)}{|\boldsymbol{r}_j - \boldsymbol{r}_i|^2}W(r_{ij},\, r_e) \\ &+ \frac{D}{n^0}\sum_{j\neq i}\frac{(P_i - P'_{i,\min})}{\rho_i}\frac{(\boldsymbol{r}_j - \boldsymbol{r}_i)}{|\boldsymbol{r}_j - \boldsymbol{r}_i|^2}W(r_{ij},\, r_e) \end{aligned} \tag{18}$$

where $P'_{i,\min}$ represents the minimal pressure among the same-phase neighboring particles around the target particle i. The first term on the right-hand side of Eq. (18) is a modified form of the original pressure gradient model, in which the inter-particle density is introduced to maintain consistency among the accelerations. The second term is in the same direction as the vector defined in Eq. (11), from the denser region to the more dilute region. Therefore, it can be regarded as a particle-stabilizing term [61] (PST) favorable for the uniform distribution of particles through the exertion of an artificial force.

3.5. Surface tension model

Although the surface tension force is less dominant in the sloshing flows, it helps keep the phase interface clear by preventing nonphysical penetrations. In the MMPS method, the continuum surface force (CSF) model proposed by Brackbill et al. [62] is used, in which the surface tension force is converted into a body force that can be calculated as:

$$\boldsymbol{F}^S = -\sigma\kappa\nabla C \tag{19}$$

where σ is the coefficient of surface tension, κ is the interface curvature, and ∇C is the gradient of a color function which can be calculated with the gradient model in Eq. (4). To maintain the continuity of accelerations, the density-weighted color function [63] is defined:

$$C_{ij} = \begin{cases} 0 & \text{if particles i and j belong to the same phase} \\ \dfrac{2\rho_i}{\rho_i+\rho_j} & \text{if particles i and j belong to different phases} \end{cases} \tag{20}$$

To calculate the interface curvature κ, the analytical method proposed in the contoured continuum surface force (CCSF) model [64] is employed here. Its main idea is to approximate the phase interface by contours of the smoothed color function. In the first step, the smoothed color function f at an arbitrary location (x, y) is obtain by the spatially weighted averaging of the original color function:

$$f(x,y) = \frac{\sum_{j\neq i} C_j G(r_{ij}, r_s)}{\sum_{j\neq i} G(r_{ij}, r_s)}, \quad G(r_{ij}, r_s) = \frac{9}{\pi r_s^2}\exp\left(-\frac{9r_{ij}^2}{r_s^2}\right) \tag{21}$$

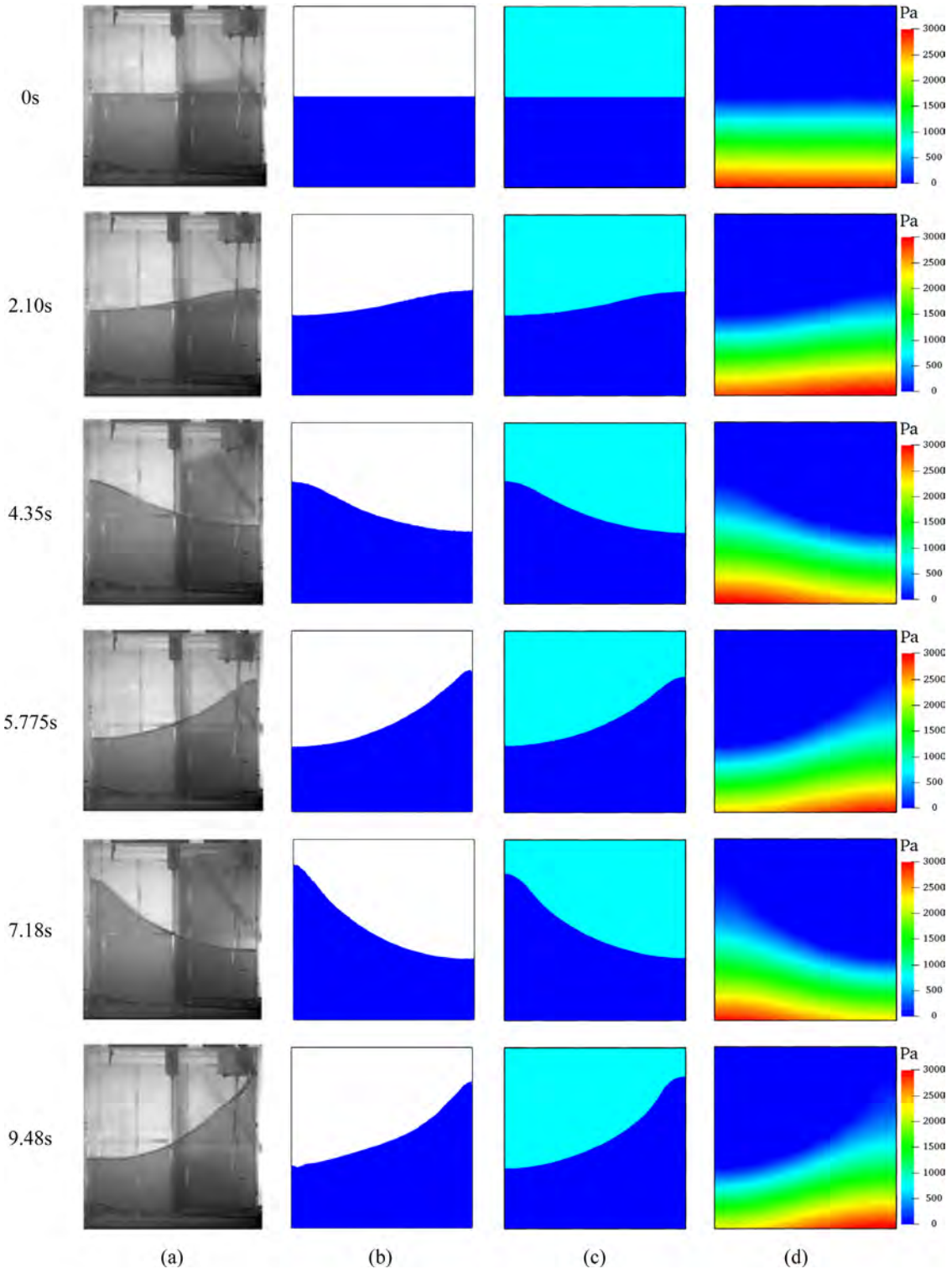

Fig. 13. Comparison of the sloshing without wave breaking between numerical and experimental [45] methods. (a) Experiment. (b) IMPS method. (c–d) Phase distribution and pressure field calculated by the MMPS method.

Then, the local contour passing through particle i can be obtained by a Taylor series expansion:

$$f_{x,i}(x-x_i)+f_{y,i}(y-y_i)+\frac{1}{2}f_{xx,i}(x-x_i)^2+f_{xy,i}(x-x_i)(y-y_i) + \frac{1}{2}f_{yy,i}(y-y_i)^2=0 \tag{22}$$

where the subscripts x and y represent partial derivatives with respect to x and y, respectively.

Finally, the curvature of the interface at particle i can be analytically calculated as:

$$\kappa_i=\frac{y''}{(1+y_i')^{3/2}}=\frac{2f_{x,i}f_{y,i}f_{xy,i}-f_{x,i}^2f_{yy,i}-f_{y,i}^2f_{xx,i}}{(f_{x,i}^2+f_{y,i}^2)^{3/2}} \tag{23}$$

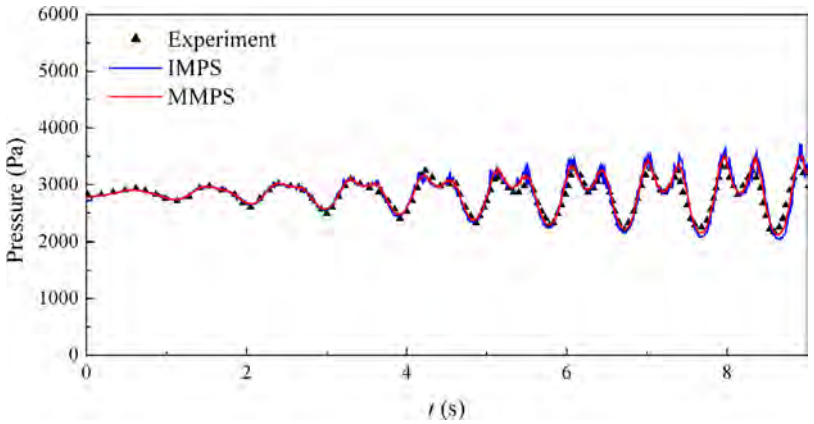

Fig. 14. Time history of impact pressures predicted by different methods in sloshing without wave breaking [45].

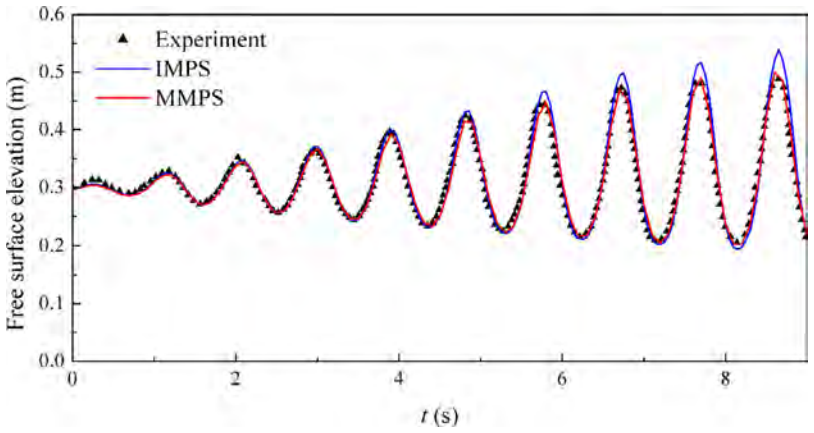

Fig. 15. Time history of wave elevations predicted by different methods in sloshing without wave breaking [45].

3.6. Multi-phase particle collision model

The uniform distribution of particles is important for the stability of MPS simulations. However, due to the randomness of their motion, the particles may get too close at some instants and nonphysical penetrations may occur. In the MMPS method, the multi-phase collision model [58], which assumes the occurrence of particle collisions in case the distance between particles is shorter than a certain threshold, is used to correct the velocities and locations of particles based on the theory of collision of two spheres with different masses. The velocities of the particles after collision are calculated as:

$$\boldsymbol{u}_i' = \boldsymbol{u}_i - \frac{1}{\rho_i}(1+\varepsilon)\frac{\rho_i\rho_j}{\rho_i+\rho_j}\boldsymbol{u}_{ij}^n \tag{24}$$

$$\boldsymbol{u}_j' = \boldsymbol{u}_j + \frac{1}{\rho_j}(1+\varepsilon)\frac{\rho_i\rho_j}{\rho_i+\rho_j}\boldsymbol{u}_{ij}^n \tag{25}$$

where $\boldsymbol{u}_i'$ and $\boldsymbol{u}_j'$ are the velocity vectors after collision, $\boldsymbol{u}_{ij}^n$ is the normal relative velocity of particles i and j, respectively, ε represents the collision ratio which is equal to 0.5 in this study, as suggested by Shakibaeinia and Jin [58].

3.7. compressible–incompressible model

In some violent cases, the compression of the air phase may be induced by the strong impact of sloshing waves on walls of the tank. To reproduce this process, the compressible–incompressible model is used in the MMPS method, in which the water and air phases are considered to be incompressible and compressible, respectively. As in case of treatments by Khayyer and Gotoh, [65,66] and Duan et al. [61] a compressibility term derived from the equation of state is included in the PPE source term of the air particles:

$$\langle\nabla^2 P^{k+1}\rangle_i = (1-\gamma)\frac{\rho}{\Delta t}\nabla\cdot\boldsymbol{u}_i^* - \gamma\frac{\rho}{\Delta t^2}\frac{\langle n^k\rangle_i - n^0}{n^0} + \frac{1}{\Delta t^2 C_s^2}P_i^{k+1} \tag{26}$$

where C_s is the physical speed of sound, equal to 340 m/s in the present study. An additional benefit of the above model is that the compressibility term can be moved to the left-hand side of Eq. (26) in the solving of PPE, which increases the values of the diagonal elements of the coefficient matrix and improves the stability of the calculated pressure [53].

4. Validations of MMPS method

In some of our previous studies, the validations of IMPS and MMPS methods have been presented from different aspects. For example, the convergence property of the IMPS method is verified by Zhang and Wan [50], and that of the MMPS method is verified by Wen et al. [57]. Meanwhile, their energy conservations are investigated through the numerical simulations of surface waves [50] and internal solitary waves [57], respectively. However, due to the greater challenge of the multi-phase simulation of violent

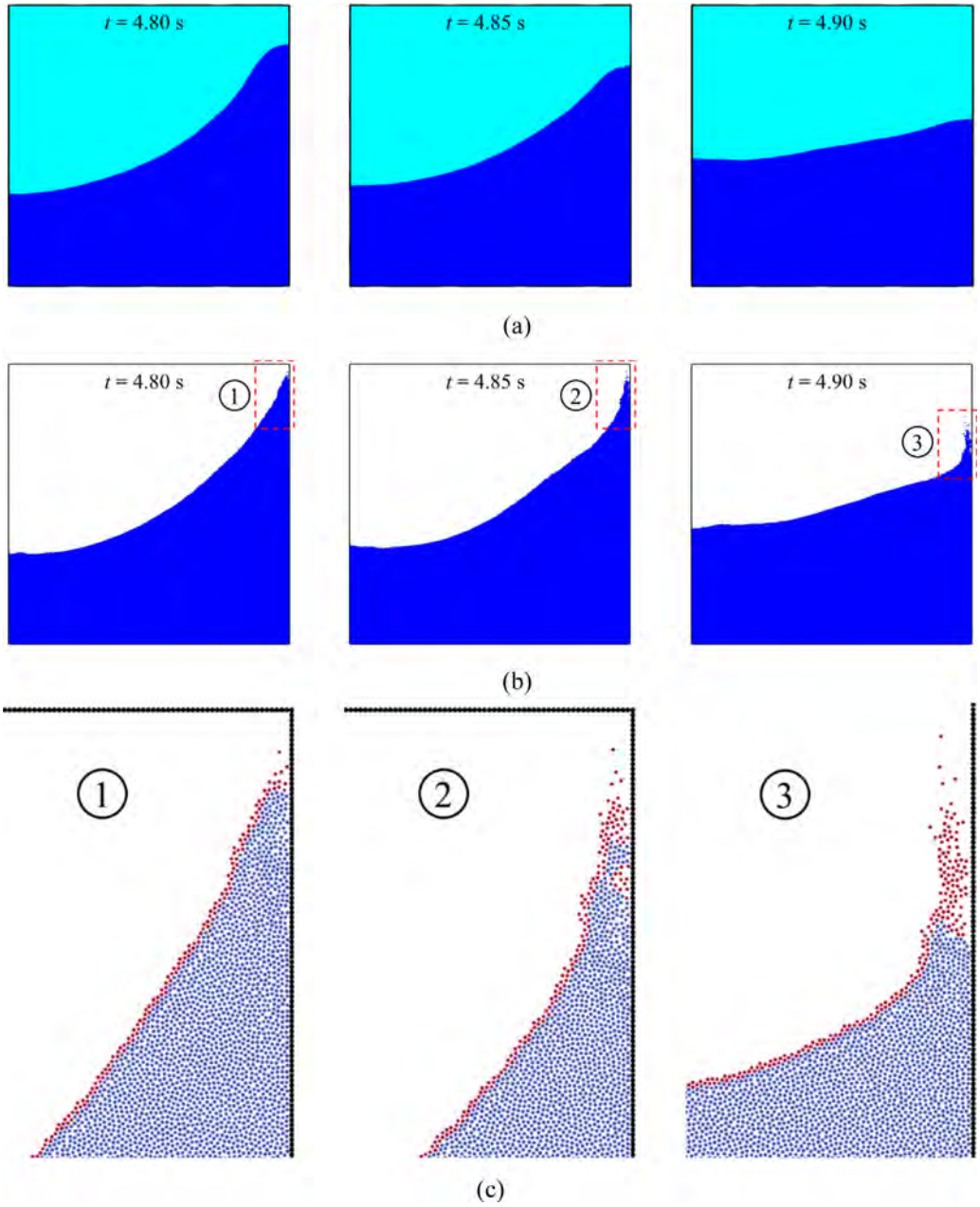

Fig. 16. Comparison of free surface treatments in different methods. (a) MMPS method. (b) IMPS method. (c) Misjudgment of free surface particles in the IMPS method.

sloshing flows, more validations of the MMPS method are still needed to be carried out.

There are two main challenges for the numerical simulations of violent sloshing flows. The first one corresponds to the instability caused by the high density ratio, which is also an important target of the above multi-phase models. The second challenge is the accurate capturing of the complex interfaces generated by the complicated phenomena in the violent sloshing flows, such as breaking waves, overturned free surface, and splashing water. In this section, the static multi-fluid system and the Rayleigh–Taylor instability are respectively simulated to validate the capacity of the MMPS method to address these two challenges.

4.1. Static multi-fluid system

As shown in Fig. 4, two immiscible fluids with the same depth of 0.75 m are poured in a 2D rectangular tank and remain completely static. The physical properties of fluids are nearly identical, except that the densities of the lower and upper fluids are 1000 kg/m^3 and 1 kg/m^3, respectively. Hence, the density ratio in this case reaches up to 1,000. The single-phase and multi-phase simulations are respectively carried out with the IMPS and the MMPS methods, then the results are compared to illustrate the improvements brought about by the multi-phase models.

Fig. 5 shows snapshots of the local particle distribution near the phase interface as simulated by the IMPS method. As it can be seen, a significant discrepancy in accelerations leads to significantly different movements of the lighter and heavier fluids, thus the lighter particles are quickly stimulated and moved up with a high acceleration that disrupts their uniform distribution. By contrast, the distribution of the heavier particles remains almost unchanged until $t = 0.03$ s. Then, the lighter particles begin to fall freely and penetrate the heavier particles at $t = 0.08$ s, disrupting the calm state of the lower fluid. Finally, blow-up instability occurs at $t = 0.2$ s.

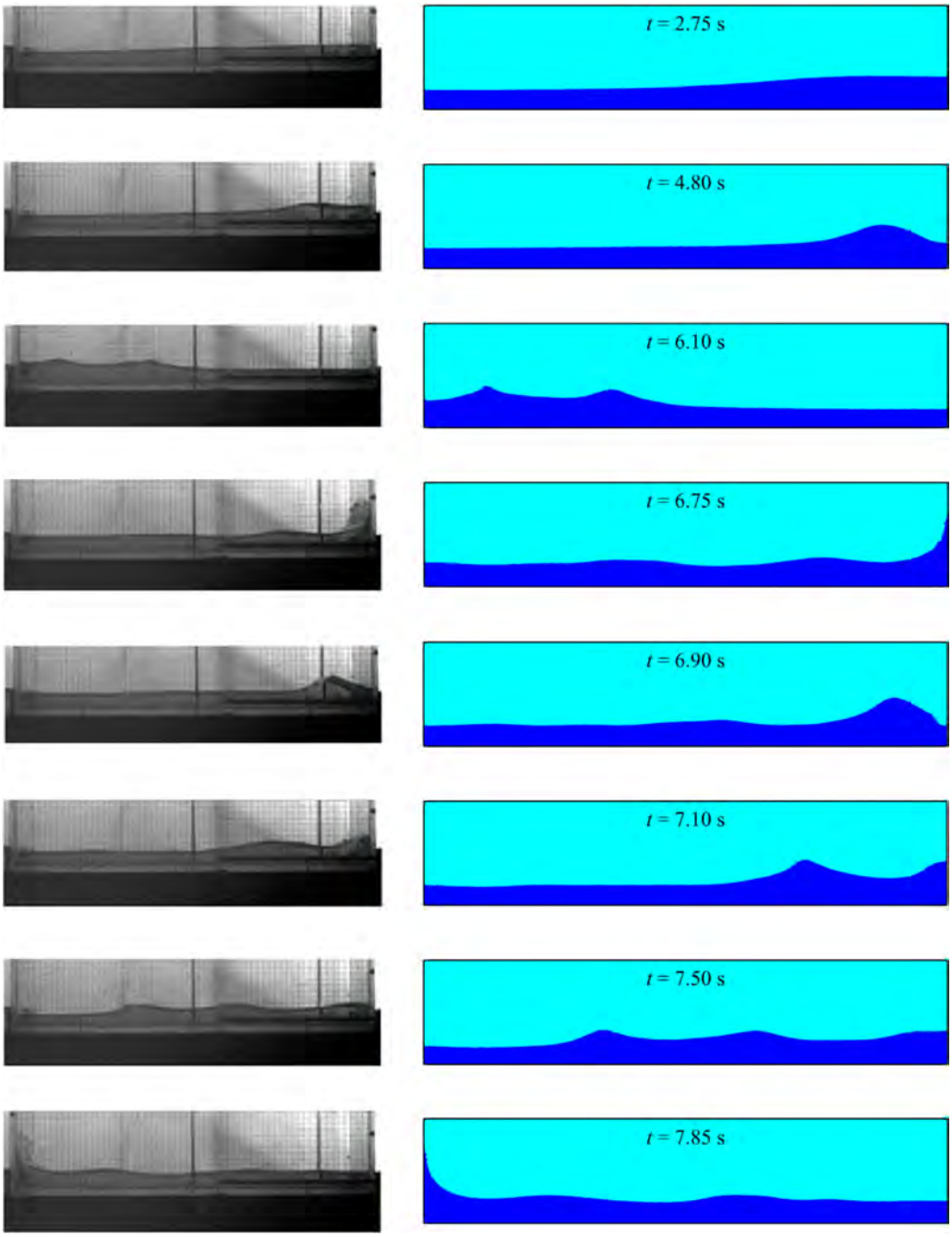

Fig. 17. Comparison of snapshots of sloshing flows with mild wave breaking between the experiment [45] (left) and the MMPS simulation (right).

Fig. 6 shows the results of the numerical simulation using the MMPS method, including the phase field, pressure field, and local particle distribution on the phase interface. Due to improvements brought by the multi-phase models, the phase field becomes stable, and the pressure field remains smooth throughout the entire simulation. Moreover, the uniform distribution of particles on both sides of the phase interface is well guaranteed. Fig. 7 compares the hydrostatic pressures calculated by the MMPS method with those of the analytical solutions. Except for a short fluctuation at the start of the simulation, the numerical results agree well with the analytical solutions at three different depths. This simple validation shows that the instability caused by the high density ratio can be adequately inhibited by the MMPS method.

4.2. Rayleigh–Taylor instability

The Rayleigh–Taylor instability (RTI) is a typical example of multi-phase flow with complex interfaces. As shown in Fig. 8, the RTI problem, which has been studied by Yang and Liu [48] as well as Hu and Adams, [67] is considered here. In a 2D rectangular tank with the dimension of 1 m $\times$2 m (width $\times$height), the heavier fluid with a density of 1.8 kg/m^3 is placed in the upper half of the container over the lighter fluid, which has a density of 1.0 kg/m^3. The viscosity of both fluids is 2.5 $\times$ 10^{-3} Pa· s and the gravitational acceleration is set to 1 m/s^2. The surface tension effect is neglected in this case. All inner walls of the tank are treated as no-slip boundary. At first, the two-phase system was

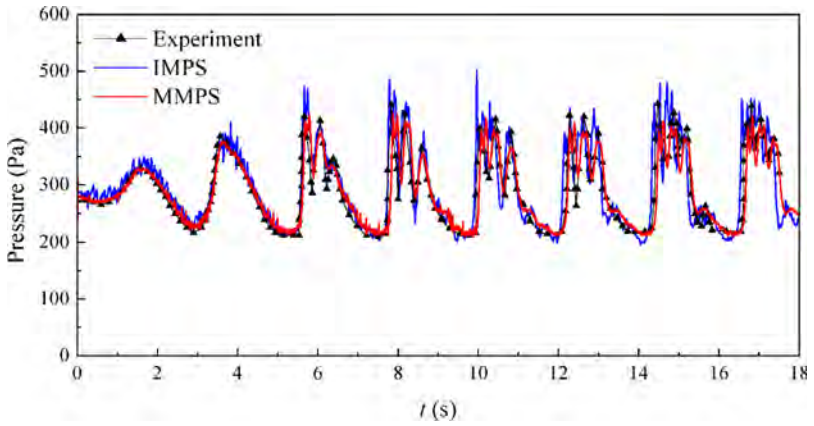

Fig. 18. Time history of the impact pressures predicted by different methods in sloshing flows with mild wave breaking [45].

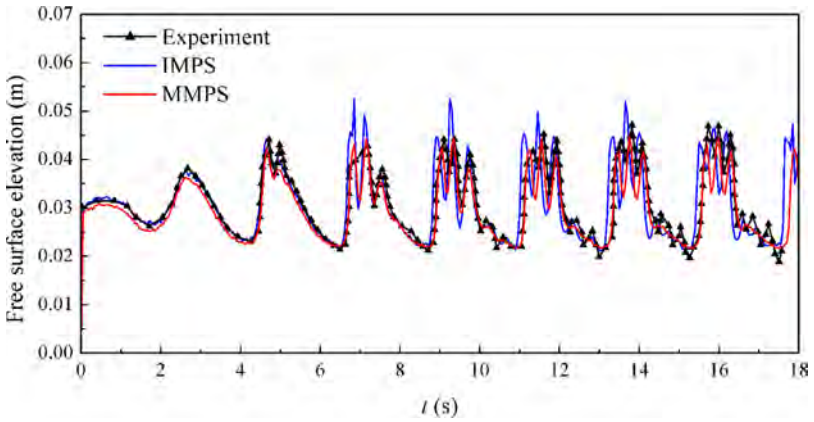

Fig. 19. Time history of wave elevations predicted by different methods in sloshing flows with mild wave breaking [45].

completely static, and a single sinusoidal disturbance is imposed on the phase interface according to $y = 1–0.15\sin(2\pi x)$.

Fig. 9 shows the evolution of the RTI as simulated by the MMPS method at $t = 0$ s, 1 s, 3 s, and 5 s. It is clear that with the continuous development of the RTI, the phase interface gradually deforms into a complex shape. Nevertheless, it is accurately captured without any nonphysical penetration observed, thus validating the numerical instability of the MMPS method. In Fig. 10, the RTI interface obtained by the MMPS method at $t = 5$ s is compared with the results of the level set [48] and the SPH[48,67] methods in the literature. The phase interfaces captured by different methods are similar, and the numerical results of the MMPS show very good agreement with those of the level set method. The nonphysical penetrations and sawtooth interface observed in the other two methods are well avoided.

Fig. 11 shows the streamline distribution and evolution of the vortices obtained by the MMPS and the SPH methods. Multiple vortices are formed with the development of the RTI, which is also the main reason for the appearance of complex interfaces. In addition, the locations and sizes of the vortices predicted by the MMPS show very good agreement with the results of the SPH. Overall, the above RTI simulation verifies the capacity of the MMPS method to capture complex interfaces owing to its meshless characteristics and the fidelity of the various multi-phase models introduced.

5. Numerical simulations and analysis

In this section, both the IMPS and the MMPS methods are applied to numerically simulate a violently sloshing liquid, and a comparative analysis is performed to illustrate the necessity of the multi-phase simulation in this context. To consider the influence of the intensity of sloshing, three cases involving increasing intensities and different forms of sloshing waves are studied: sloshing without wave breaking, sloshing with mild wave breaking, and sloshing with violent wave breaking. In order to compare the results of single-phase and multi-phase simulations, the numerical parameters adopted by the IMPS and the MMPS methods keep identical in the same case, such as the time step, the particle size and so on.

All the simulations are completed on the GPU (Graphics Processing Unit) device to improve the computational efficiency. In the study of Chen and Wan [68,69], the combination of the IMPS method and the GPU acceleration technology has been realized and introduced in detail. Due to the simultaneous solution of different phase, the calculation process of MMPS remains to be consistent with that of IMPS method, except for the addition of multi-phase models which will not cost too much computing time. Thus, the speedup of GPU for multi-phase simulation can be considered as almost the same as that in single-phase simulation.

5.1. Case 1: Sloshing without wave breaking

The numerical model shown in Fig. 12 is used to simulate the sloshing without wave breaking, which keeps consistent with the experimental model adopted by Koh et al. [45] A 2D rectangular tank with the width and height of 0.6 m is disturbed to horizontal harmonic motion. The equation of motion is $x = -A(1 - \cos\omega t)$, where $A = 0.005$ m is the amplitude of excitation and ω = 6.85 rad/s is the angular frequency of excitation. The density and

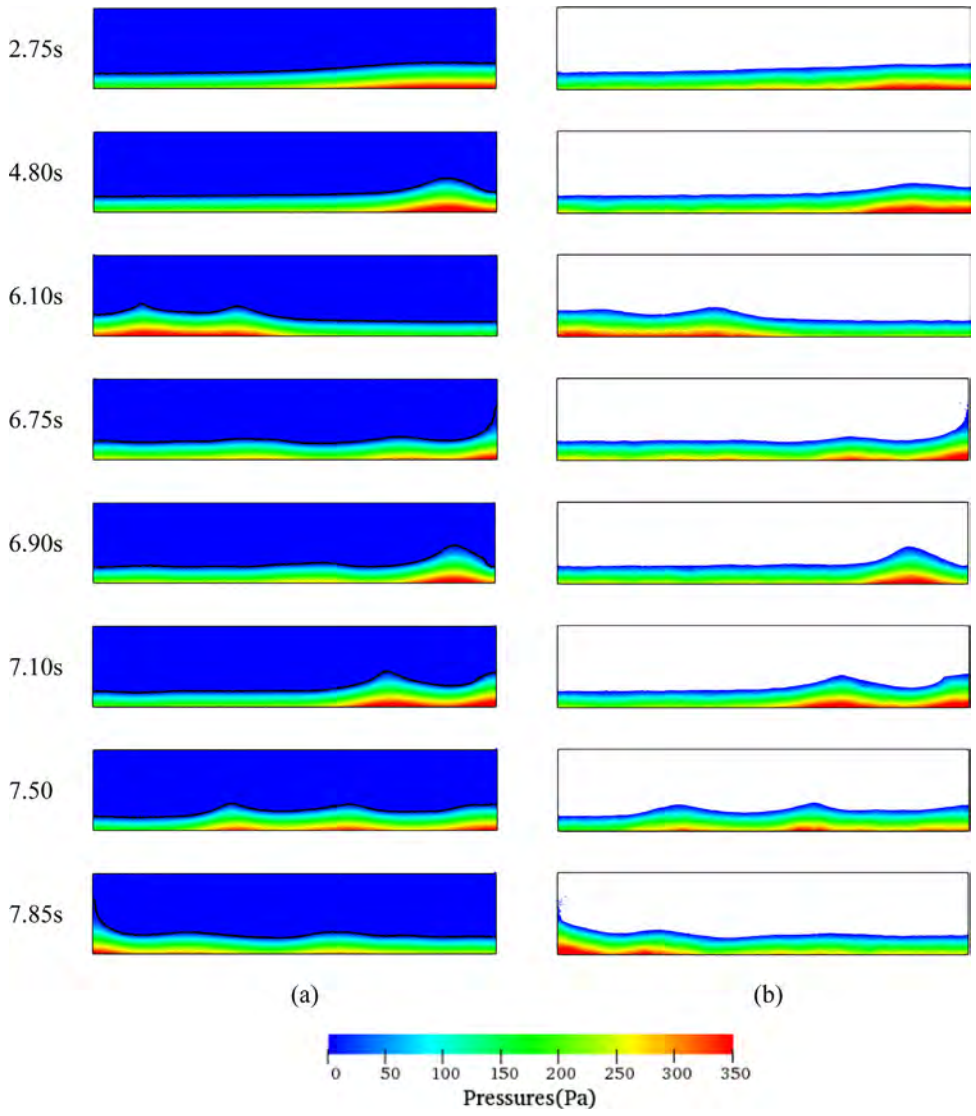

Fig. 20. Comparison of pressure fields calculated by different methods. (a) MMPS method. (b) IMPS method.

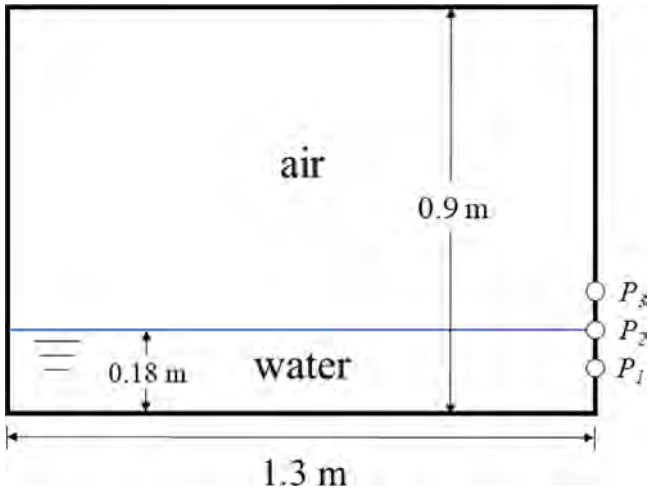

Fig. 21. Numerical model of the sloshing with violent wave breaking.

viscosity of the water phase are 1×10^3 kg/m^3 and 1×10^{-3} Pa·s, and those of the air phase are 1.29 kg/m^3 and 1.5×10^{-5} Pa·s, respectively. The coefficient of surface tension is 7.27×10^{-3} N/m. In this case, a high water filling rate of 50% is adopted, thus

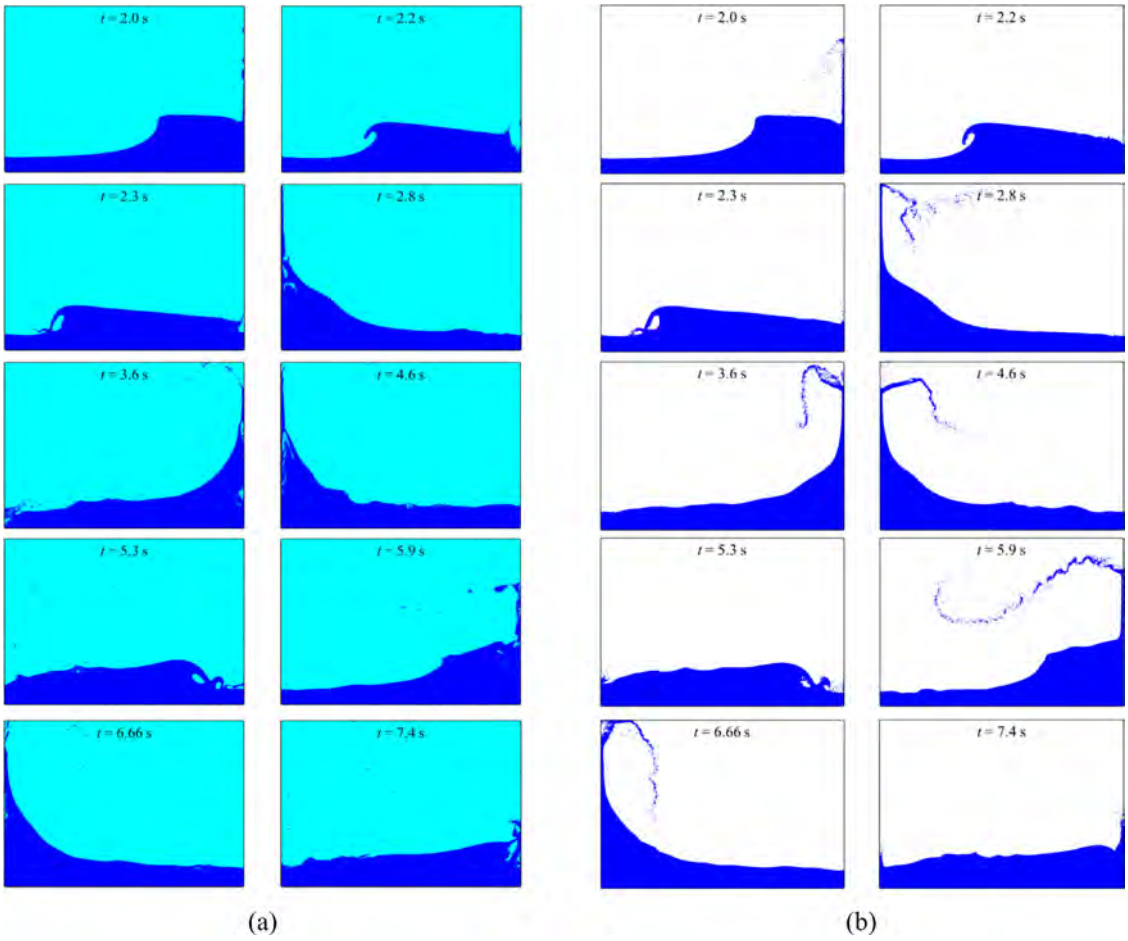

Fig. 22. Snapshots of sloshing with violent wave breaking simulated by different methods. (a) MMPS method. (b) IMPS method.

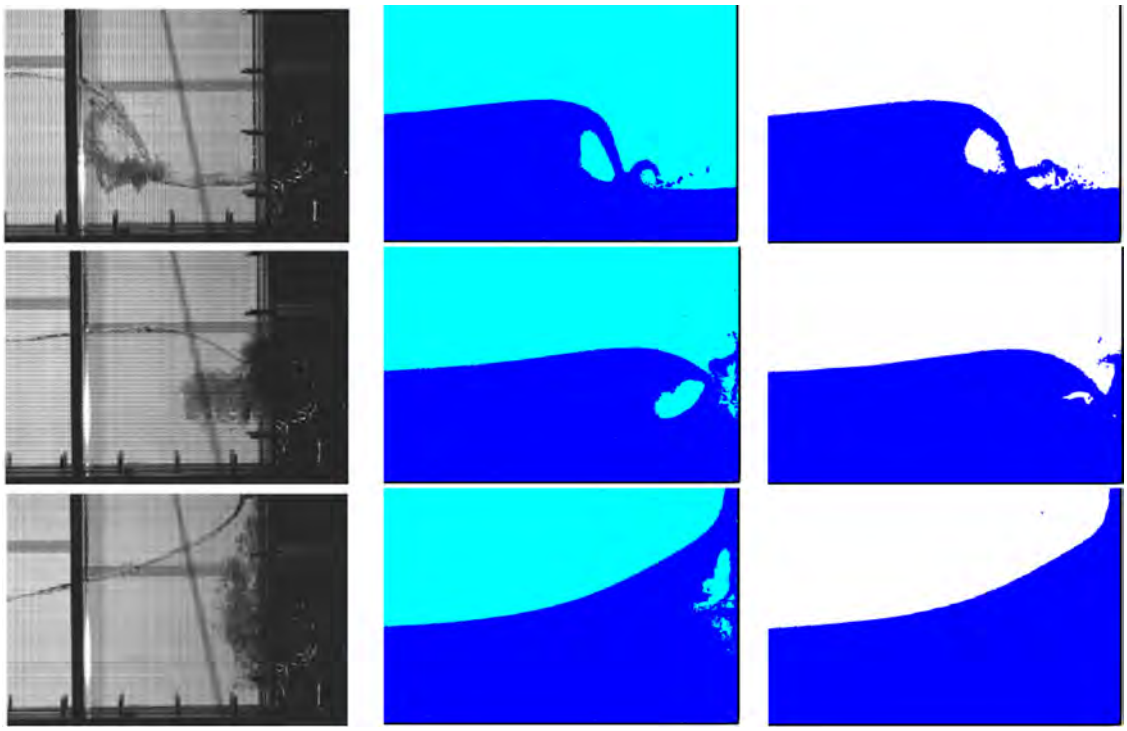

Fig. 23. Air entrapment and cavity evolution as captured in the experiment [59] (left), MMPS simulation (middle), and IMPS simulation (right).

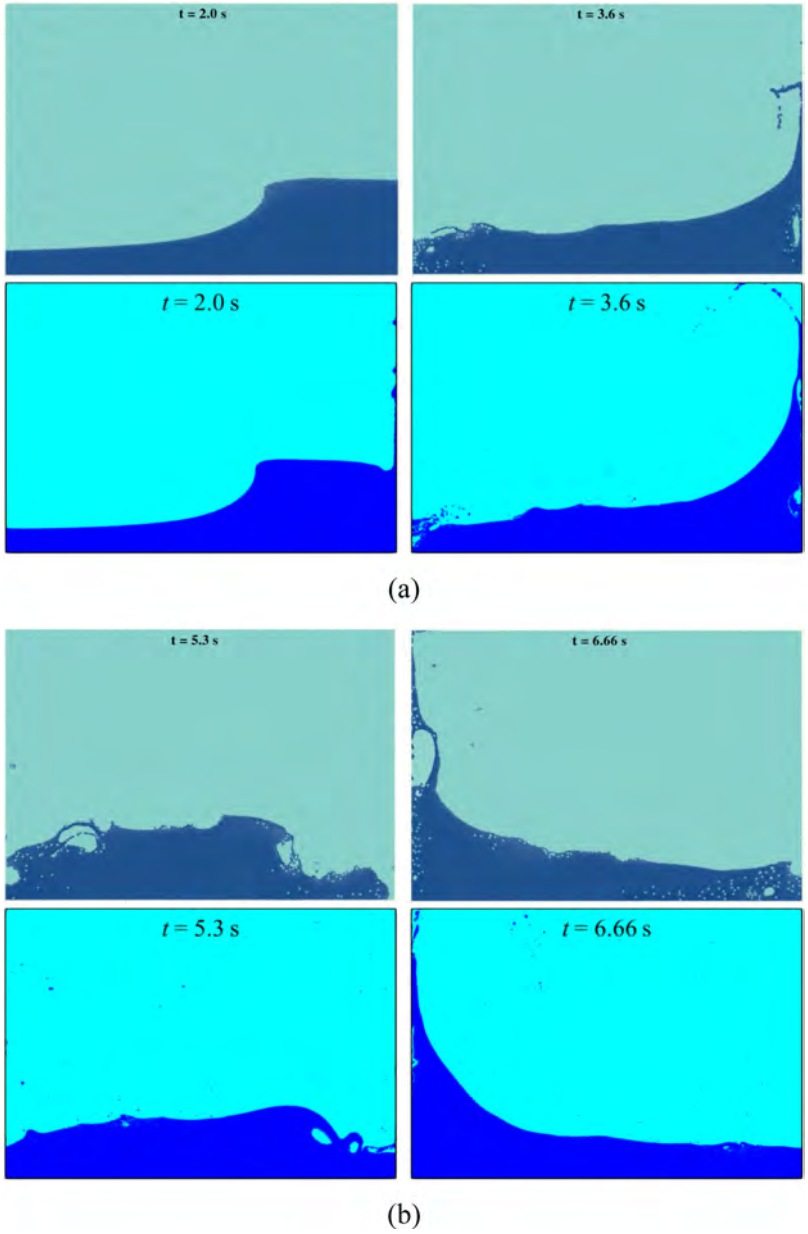

Fig. 24. Comparison of phase interfaces captured by the SPH [60] (top) and MMPS methods (bottom). (a) Results of simulation in the early stage and (b) the later stage.

the depth is equal to 0.3 m. A pressure probe P_1 is arranged on the left wall of the tank at a distance of 0.02 m from the bottom, and a wave probe P_2 is fixed 0.02 m from the right wall of the tank. The numerical simulation is conducted with an initial particle spacing of 0.001 m and a fixed time step of 0.0001 s.

Fig. 13 shows the evolution of the sloshing without wave breaking as simulated by the IMPS and the MMPS methods as well as the snapshots obtained in the experiment. [45] A sloshing wave with a large amplitude is formed due to the swaying motion of the tank, and it leads to the acute deformation of the phase interface. However, although the sloshing flow is violent, the phenomenon of wave breaking is still not observed and the shape of phase interface is not complex. A good agreement between the numerical and the experimental results can be observed in terms of the shape of phase interface, and no prominent discrepancy is noted in the results of the IMPS and the MMPS, indicating that the effect of the air phase is not significant in this case. The pressure field obtained by the MMPS keeps stable and smooth throughout the simulation, validating the accuracy and stability of the MMPS in simulating problems involving violently sloshing liquid.

Figs. 14 and 15 show the comparisons of the quantitative results obtained by the IMPS and the MMPS methods with the experimental data. [45] In Fig. 14, the historical curves of impact pressure show that the results obtained by these two methods are almost entirely consistent with the experimental data. In Fig. 15, the wave elevations predicted by the IMPS and MMPS methods showed good agreement with the experimental data in the first half of the simulation. However, a significant difference emerges with the continuous development of the sloshing flow, whereby the peak amplitudes of wave elevation calculated by the IMPS method are much larger than the results of the MMPS and the experiment after $t = 5$ s.

To analyze the cause of the above difference, Fig. 16(a) and Fig. 16(b) show the processes of climbing and falling of the water head as simulated by the MMPS and the IMPS methods, respectively. The morphological difference in sloshing waves mainly

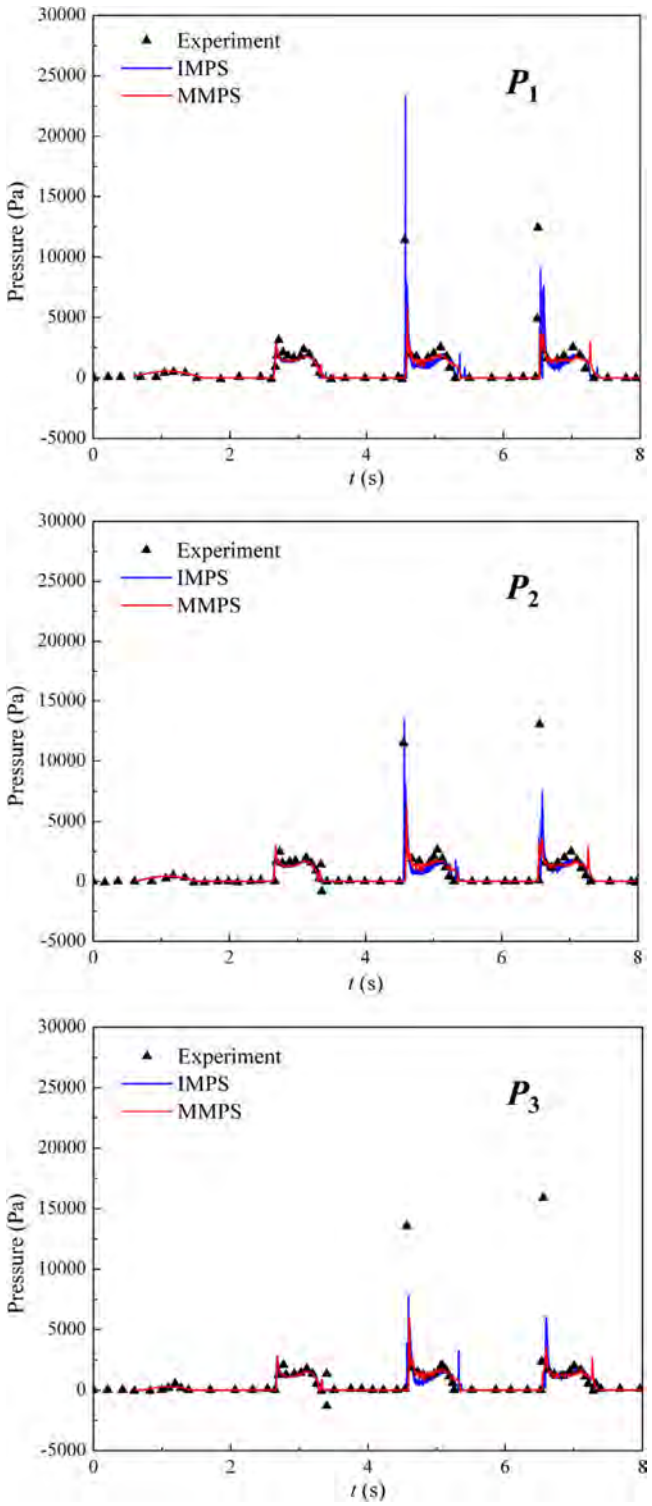

Fig. 25. Time history of impact pressures predicted by different methods in sloshing without wave breaking, and a comparison with experimental data [59].

appears near the highest point. The sloshing wave is flatter in the MMPS simulations while a sharper wave is predicted by the IMPS method, with some splashed water particles observed. The former can be attributed to the use of the surface tension model in the MMPS method. During the climbing of the water head, the sharpness and curvature of the interface of sloshing waves near the right wall of the tank increases rapidly, producing a surface tension force directed inside the water. This reduces the sharpness of the wave. However, the surface tension force is not considered in the IMPS method, because of which the growth of wave sharpness is less constrained and its calculated elevation is higher than that in the experimental data.

The splashing phenomenon in the single-phase simulation can be explained by the results of judgment of the free surface particles, as shown in Fig. 16(c). A few internal fluid particles near the free surface are misjudged as free surface particles due to the oscillation in the particle number density induced by violent sloshing. These particles are incorrectly assigned zero pressure, because of which the pressure gradient forces between these particles are ignored and inertial motion is simulated that leads to the particles splashing. In contrast to the IMPS method, the pressures of the free surface particles are calculated by solving the PPE in the MMPS method, and thus the above problem is avoided.

The above analysis shows that although the MMPS method could accurately simulate violent sloshing in this case, similar results are obtained by the IMPS method. Due to the absence of the surface tension model and the misjudgment of free surface particles, some defects are observed in the single-phase simulation. However, these defects can be solved by further improving the IMPS method. For example, a surface tension model applicable to single-phase flows has been proposed by Nomura et al. [70] A virtual particle model has also been developed, [71–73] in which the pressures of the free surface particles can be better considered by compensating for virtual particles outside the free surface. Therefore, the multi-phase simulation of sloshing without wave breaking seems to be not necessary.

5.2. Case 2: Sloshing with mild wave breaking

The model in Fig. 12 is also used to simulate a sloshing liquid with mild breaking waves, but at a low water filling rate of 5%. To obtain a higher intensity of sloshing, the amplitude of excitation A is increased to 0.01 m and the angular frequency of excitation ω is set to 2.825 rad/s, close to the first-order natural frequency of the tank. This results in resonance.

Fig. 17 shows the typical wave profiles at several time instants and a comparison with the experimental pictures. [45] Note that only the lower part of the tank is shown because of the low water filling rate used in this case. At $t = 2.75$ s, the sloshing wave is first observed as a standing wave. It then develops into a traveling wave with a single peak at $t = 4.80$ s. At $t = 6.10$ s, the second peak appears. The multi-crested wave subsequently travels in the tank and repeatedly strikes its walls. At $t = 7.85$ s, water runs up along the left wall and the wave breaks. Although the sloshing flow becomes more violent due to the resonance phenomenon and the deformation of phase interface is more complex, the MMPS method still obtains results consistent with those of the experiment.

Figs. 18 and 19 present the quantitative results obtained by the IMPS and the MMPS methods as well as the comparison with the experimental data. [45] Because the sloshing wave has complicated double wave peaks, multiple peaks occur in each period after $t = 6$ s, making the trends of the impact pressure and wave elevation difficult to be predicted. As in case 1, the wave elevation is overestimated in the single-phase simulation. Moreover, the peak amplitude of the impact pressure is also overestimated by the IMPS method in this case, indicating that the effect of the air phase has increased with the intensity of sloshing, and the accuracy of the calculated pressure in the single-phase simulation has thus decreased. The results of calculation of the MMPS method still agree well with the experimental data, but the peak values tend to be lower than those in the experiment. Considering that the MMPS results keep quite consistent with

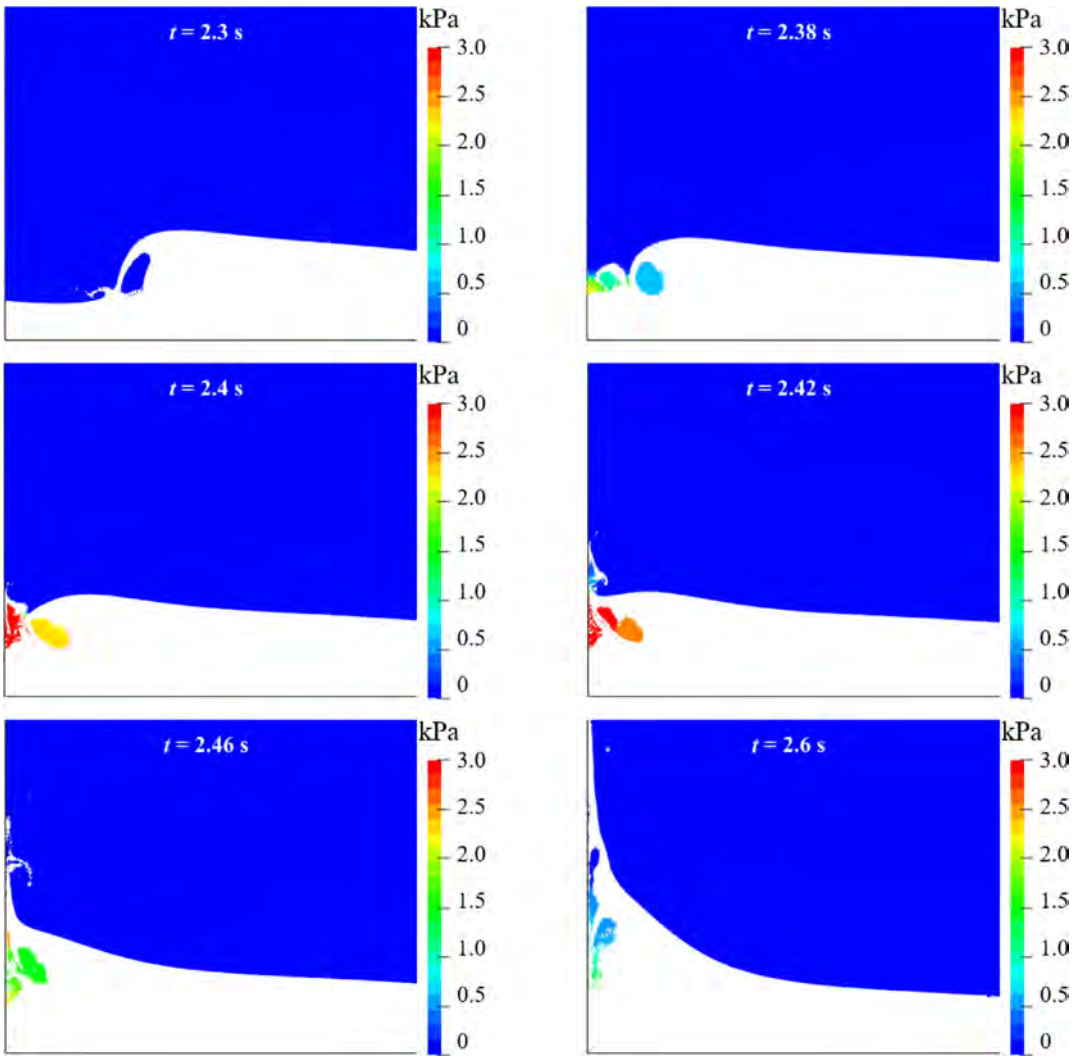

Fig. 26. Evolutions of shape and pressure inside the air cavity during impact by sloshing with violent wave breaking.

experimental results in case 1, the main reason for the difference should be the increase of sloshing intensity which brings huge difficulties for numerical methods.

Fig. 20 shows the comparison of the pressure fields obtained by the IMPS and the MMPS methods at different instants, and a good agreement with the experimental data can be observed. However, the pressure field near the wall of the tank is slightly larger in the single-phase simulation during the impact at 6.75 s and 7.85 s, which is consistent with the quantitative results in Fig. 19. To sum up, the increase in the intensity of sloshing and the stronger air effect causes the results of simulation by the IMPS and the MMPS methods to be more different from each other in this case. Therefore, although the single-phase simulation still obtains similar results to those of the experiment, the improvements brought about by the multi-phase simulation are verified to some degree.

5.3. Case 3: Sloshing with violent wave breaking

Although the sloshing flows are violent, the intensities of sloshing in the above two cases are still not comparable to that in the extreme ocean conditions. In this section, a sloshing liquid with violent wave breaking is further considered by using the experimental model of Rafiee et al. [59], as shown in Fig. 21. The width and height of the 2D tank are 1.3 m and 0.9 m, respectively, and a water filling rate of 20% is chosen. The motion of tank follows $x = A\sin(2f_0\pi t)$, where $A = 0.1$ m and $f_0 = 0.496$ s^{-1}, close to the first-order natural frequency of the tank. The physical properties of water and air are the same as in the model of Fig. 12. Three pressure probes—P_1, P_2, and P_3—are arranged on the right wall of the tank, and are 0.165 m, 0.18 m, and 0.195 m from the bottom, respectively. Numerical simulation is conducted with the initial particle spacing of 0.002 m and the fixed time step of 0.0001 s.

Fig. 22 shows several typical snapshots of the sloshing flows simulated by the IMPS and the MMPS methods. The comparison shows that before $t = 2.3$ s, the profiles of sloshing waves keep identical in these two simulations. At $t = 2.3$ s, the overturned free surface impacts the underlying water, causing the formation of an air cavity. In the single-phase simulation, the air cavity is assumed to be an empty area as the air phase is ignored in the IMPS method. Therefore, the internal space of the cavity is quickly occupied by water particles in the subsequent impact, and the cavity soon disappears. By contrast, the cavity consists of the real air particles in the multi-phase simulation, thus although the cavity is subjected to severe deformation, it does not disappear unphysically, and the entrapped air has a significant influence on the evolution of the sloshing waves. Moreover, when the splashed water particles fall back into the underlying water, some air particles are entrapped in the region below the free surface. This

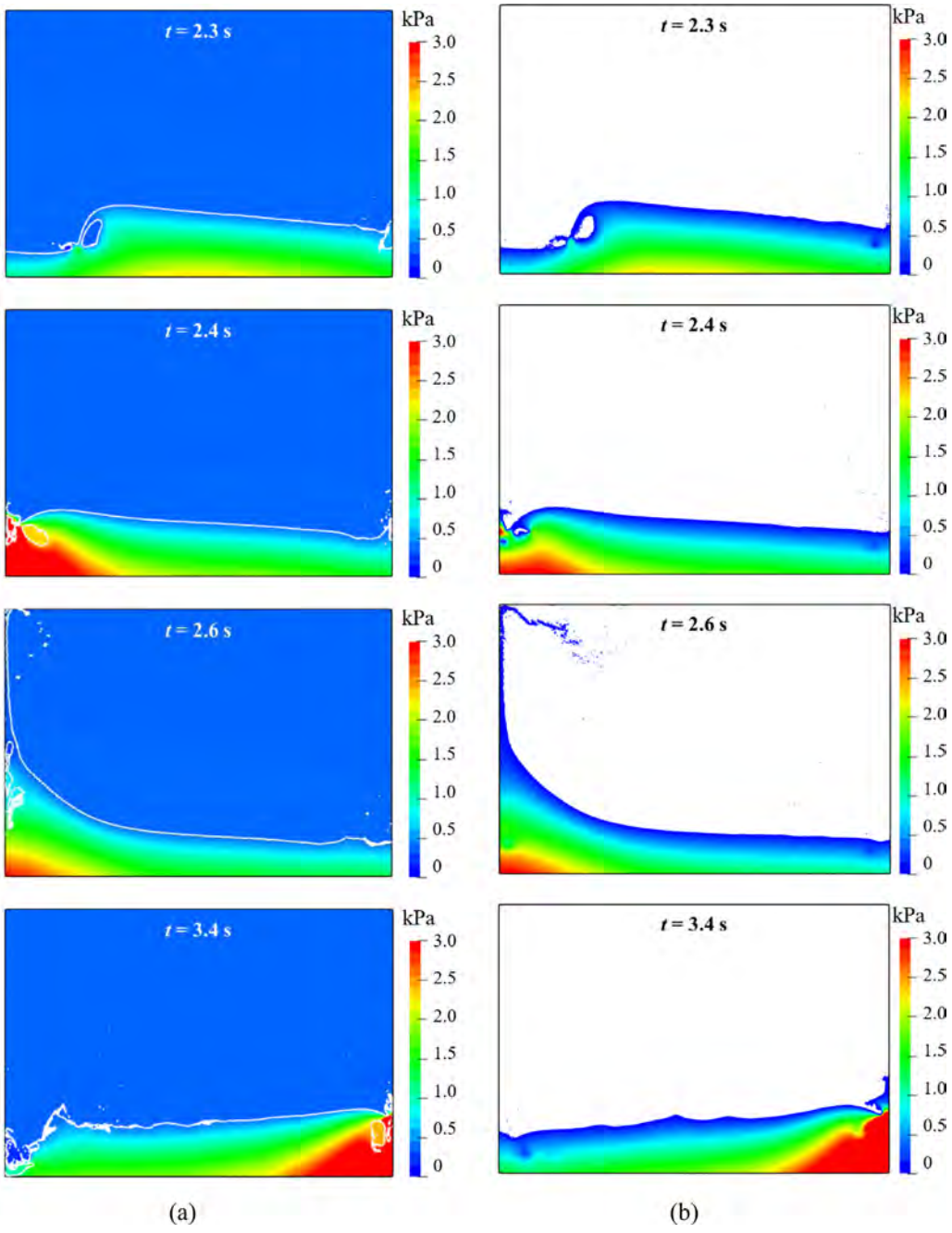

Fig. 27. Pressure fields calculated by different methods at four instants in sloshing with violent wave breaking. (a) MMPS method. (b) IMPS method.

is precisely simulated by the MMPS method and ignored by the IMPS method.

Fig. 23 shows the phenomenon of air entrapment captured by the MMPS, IMPS, and experimental methods. [59] The locations and shapes of the cavity predicted by the MMPS method are in good agreement with those of the experiments at different instants, through which the capacity of the MMPS method to represent violent sloshing in case of air entrapment is validated. On the contrary, although it is able to predict the formation of the cavity, the IMPS method could not reproduce the whole evolution of the cavity during impact. Therefore, the necessity of multi-phase simulations to model sloshing flows that are sufficiently violent to cause breaking waves and air entrapment is verified.

Fig. 24 shows the comparison of the phase interfaces captured by the MMPS and SPH [60] methods. In the early stage of the simulation, good agreement is achieved between these two methods. However, the interface captured by the MMPS is more natural and clearer than the SPH later in the simulation, possibly because of the different fluid viscosities set. In the SPH method, the artificial viscosity is much larger than the real viscosity of the fluid, and is used to enhance numerical stability. The real viscosity of the fluid is directly applied in the MMPS simulation, which benefits from the improved stability brought about by the semi-implicit algorithm. In this case, the sloshing waves repeatedly impact the walls of the tank and cause the violent mixing of water and air. At the same time, a separation occurs due to the buoyancy

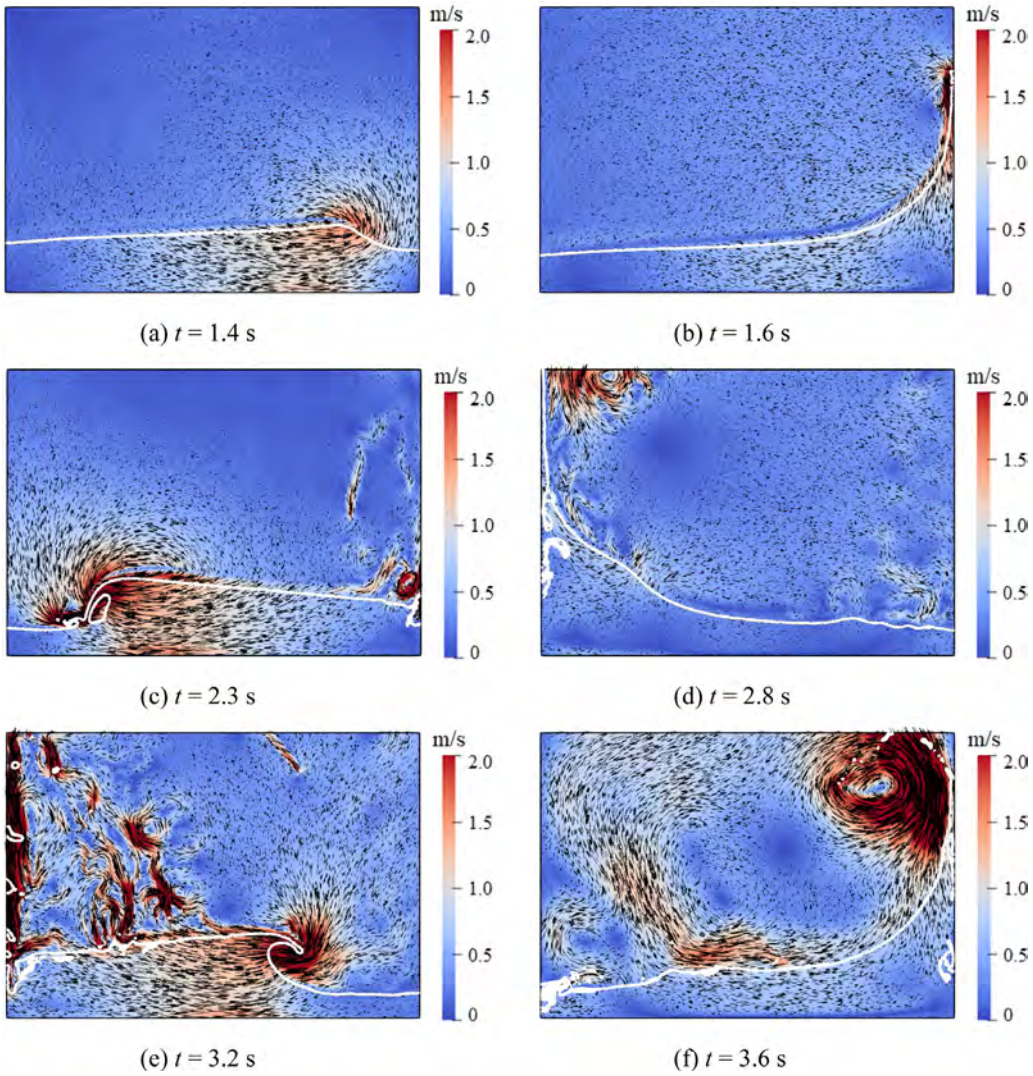

Fig. 28. Velocity field and velocity vectors obtained in the MMPS simulation.

effect between successive impacts on the same sidewall, and the trapped air gradually emerges from the free surface. When artificial viscosity is used, the separation process is weakened, and the degree of mixing increases continuously to result in an unclear interface in the SPH simulation. By using the real viscosity of the fluid, the MMPS method is able to better consider both the mixing and separation processes, and thus could accurately capture the phase interface even after the long-term evolution of the sloshing flows.

Fig. 25 shows the time history of the impact pressures calculated by the IMPS and the MMPS methods, and recorded by the three probes, as well as their comparison with the experimental data. [59] Good agreement between the numerical and experimental results is observed in the global shape of the pressure history, with the secondary impact at each cycle well reproduced by both the IMPS and the MMPS methods. The impact pressure in violent sloshing flow is stochastic; thus, it seems to be less possible to obtain a perfect agreement between the numerical and experimental results. A comparison of the results of the IMPS and MMPS shows that the peak pressure values predicted by the MMPS method are much lower than those predicted by the IMPS at all three probes, implying that the trapped air cavity has a significant cushioning effect on the process of impact.

To better illustrate the cushioning effect of air, Fig. 26 shows the evolutions of the shape and pressure of the air cavity during the whole process of impact. The air cavity is continuously compressed by the approaching sloshing wave to the wall of the tank, leading to a rapid increase in cavity pressure. In this process, a mass of wave energies is dissipated; thus, the impact is weakened, and the impact pressure decreases. However, the above compression process could not be reproduced in the single-phase simulation because the cushioning effect of air is ignored, and the impact pressure predicted by the IMPS method is thus significantly overestimated.

Fig. 27 shows the pressure fields obtained by the IMPS and the MMPS methods. It is clear that the stability and smoothness of the pressure field is well maintained in both the single-phase and the multi-phase simulations. However, when the cavity persists in the single-phase simulation ($t = 2.3$ s and $t = 2.4$ s), the water particles along its edge are misjudged as free surface particles and assigned zero pressure. This results in a nonphysical pressure field around the cavity. By contrast, the cavity pressure

is fully considered by the MMPS method, and a notable pressure gradient between the air cavity and the surrounding water is observed. Moreover, the smooth transition of the pressure field across the phase interface is achieved, with no oscillations in pressure observed.

Fig. 28 shows the velocity field obtained by the MMPS method together with the velocity vectors. Although the amplitudes of velocities of water and air are comparable, considerably more complex flow structures are generated in the region occupied by air. During the propagation of sloshing waves, the vortical motion of the air particles occurs near the wave front ($t = 1.4$ s), which becomes violent when the wave overturns and some air particles quickly escapes from the open cavity ($t = 2.3$ s and $t = 3.2$ s). Affected by the wave run-up, another vortex structure with a large radius is observed above the sloshing wave ($t = 3.6$). Moreover, when the splashed water particles fall freely, multiple and small vortical structures are generated in the air region, disturbing the flow field severely ($t = 3.2$ s). The accurate representation of the above complicated phenomena verifies the capacity of the MMPS method.

6. Conclusions

Based on the IMPS and the MMPS methods, a set of problems involving liquids sloshing with different intensities are simulated in this paper, and the necessity of the multi-phase simulation is illustrated through a comparative study. The following conclusions can be drawn from the work here:

(1) By introducing various multi-phase models to the IMPS method, the MMPS method is developed and presented in detail. Its capacity to deal with a high density ratio and complex phase interfaces, which are the main challenges to the numerical simulation of violent sloshing flows, is verified through the successful simulation of the static multi-fluid system and the Rayleigh–Taylor instability, respectively.

(2) The global and local features of violent sloshing flows are adequately reproduced by the MMPS method, and the qualitative and quantitative results are generally in very good agreement with those of experiments. However, some discrepancies in the peak pressure values might have been caused because the 3D effect in case of violent wave breaking is ignored. This is a direction for future work to be pursued by the authors. Compared with the SPH method, the MMPS method can better consider the mixing and separation processes induced by wave breaking. It does so by using the real viscosity of the fluid rather than artificial viscosity. Therefore, a natural and clear phase interface can be obtained by the MMPS method even after the long-term evolution of sloshing flow.

(3) A comparative study shows that when the sloshing flow is violent but does not feature breaking waves, the results of simulations of the IMPS and MMPS methods are in good agreement. Therefore, the single-phase simplification of sloshing flows, which has been used in most previous MPS studies, seems to be reasonable under this condition. However, the absence of a surface tension model and the misjudgment of free surface particles reduces the accuracy of the single-phase MPS simulation.

(4) The difference between the results of simulation of the IMPS and the MMPS methods becomes significant with the increase in the intensity of sloshing and the occurrence of breaking waves. Although the air cavity is observed in both simulations, only the MMPS method is able to predict its evolution and obtain exact profiles of the sloshing waves. The cushion effect of air is ignored in the single-phase simulation, which leads to the overestimation of peak pressure values and inaccurate representation of the pressure field around the cavity. Thus, the multi-phase simulation is necessary.

Declaration of competing interest

The authors declare the following financial interests/personal relationships which may be considered as potential competing interests: Decheng Wan reports financial support was provided by Shanghai Jiao Tong University.

Data availability

The data that support the findings of this study are available from the corresponding author upon reasonable request.

Acknowledgments

This work was supported by National Natural Science Foundation of China (Grant No. 51879159, 52131102), National Key Research and Development Program of China (2019YFB1704200), to which the authors are most grateful.

References

[1] O.F. Rognebakke, O.M. Faltinsen, Coupling of sloshing and ship motions, J. Ship Res. 47 (3) (2003) 208–221.
[2] S. Mitra, C.Z. Wang, J.N. Reddy, B.C. Khoo, A 3D fully coupled analysis of nonlinear sloshing and ship motion, Ocean Eng. 39 (2012) 1–13.
[3] W. Zhao, J. Yang, Z. Hu, L. Tao, Coupled analysis of nonlinear sloshing and ship motions, Appl. Ocean Res. 47 (2014) 85–97.
[4] Z.J. Wei, O.M. Faltinsen, C. Lugni, Q.J. Yue, Sloshing-induced slamming in screen-equipped rectangular tanks in shallow-water conditions, Phys. Fluids 27 (2015) 032104.
[5] M.G. Seo, Y. Kim, D.M. Park, Effect of internal sloshing on added resistance of ship, J. Hydrodyn. 29 (1) (2017) 13–26.
[6] X.Y. Cao, L. Tao, A.M. Zhang, F.R. Ming, Smoothed particle hydrodynamics (SPH) model for coupled analysis of a damaged ship with internal sloshing in beam seas, Phys. Fluids 31 (2019) 032103.
[7] Y.L. Li, R.C. Zhu, G.P. Miao, J. Fan, Simulation of tank sloshing based on openfoam and coupling with ship motions in time domain, J. Hydrodyn. 24 (03) (2012) 450–457.
[8] B. Bouscasse, A. Colagrossi, A. Souto-Iglesias, J.L. Cercos-Pita, Mechanical energy dissipation induced by sloshing and wave breaking in a fully coupled angular motion system. I. Theoretical formulation and numerical investigation, Phys. Fluids 26 (2014) 033103.
[9] Y. Zhuang, D.C. Wan, Numerical study on ship motion fully coupled with LNG tank sloshing in CFD method, Int. J. Comp. Meth.-Sing 16 (6) (2019) 1840022.
[10] Y. Zhuang, D.C. Wan, Numerical simulation of ship motion fully coupled with sloshing tanks by naoe-FOAM-SJTU solver, Eng. Comput. 36 (8) (2019) 2787–2810.
[11] J.J. Stephen, S.A. Sannasiraj, V. Sundar, Numerical modeling of nonlinear sloshing of liquid in a container coupled with barge subjected to regular excitation, J. Hydrodyn. 31 (5) (2019) 999–1010.
[12] P.J. Ming, W.Y. Duan, Numerical simulation of sloshing in rectangular tank with VOF based on unstructured grids, J. Hydrodyn. 22 (6) (2010) 856–864.
[13] A. Khayyer, H. Gotoh, Enhancement of stability and accuracy of the moving particle semi-implicit method, J. Comput. Phys. 230 (2011) 3093–3118.
[14] C.H. Hu, M.M. Kamra, An unstructured mesh method for numerical simulation of violent sloshing flows, J. Hydrodyn. 32 (2) (2020) 259–266.
[15] S. Koshizuka, H. Tamako, Y. Oka, A particle method for incompressible viscous flow with fluid fragmentation, Comput. Fluid Dyn. J. 4 (1) (1995) 29–46.
[16] S. Koshizuka, Y. Oka, Moving-particle semi-implicit method for fragmentation of incompressible fluid, Nucl. Sci. Eng. 123 (1996) 421–434.
[17] S. Koshizuka, A. Nobe, Y. Oka, Numerical analysis of breaking waves using the moving particle semi-implicit method, Int. J. Numer. Meth. Fluids 26 (1998) 751–769.
[18] R.A. Gingold, J.J. Monaghan, Smoothed particle hydrodynamics-theory and application to non-spherical stars, Mon. Not. R. Astron. Soc. 181 (1977) 375–389.
[19] L.B. Lucy, A numerical approach to the testing of the fission hypothesis, Astrophys. J. 82 (1977) 1013–1024.
[20] M. Luo, C.G. Koh, M. Gao, W. Bai, A particle method for two-phase flows with large density difference, Internat. J. Numer. Methods Engrg. 103 (2015) 235–255.
[21] M. Luo, C.G. Koh, W. Bai, M. Gao, A particle method for two-phase flows with compressible air pocket, Internat. J. Numer. Methods Engrg. 108 (2016) 695–721.

[22] M. Luo, A. Khayyer, P.Z. Lin, Particle methods in ocean and coastal engineering, Appl. Ocean Res. 117 (2021) 102734.
[23] H. Gotoh, A. Khayyer, Y. Shimizu, Entirely lagrangian meshfree computational methods for hydroelastic fluid–structure interactions in ocean engineering—reliability, adaptivity and generality, Appl. Ocean Res. 115 (2021) 102822.
[24] L. Zou, J.Z. Sun, Z. Sun, Z.B. Yu, H.B. Zhao, Study of two free-falling spheres interaction by coupled SPH-DEM method, Eur. J. Mech. B-Fluid 92 (2022) 49–64.
[25] M. McLoone, N.J. Quinlan, Coupling of the meshless finite volume particle method and the finite element method for fluid–structure interaction with thin elastic structures, Eur. J. Mech. B-Fluid 92 (2022) 117–131.
[26] C. Pilloton, A. ardazzi, A. olagrossi, S. Marrone, SPH method for long-time simulations of sloshing flows in LNG tanks, Eur. J. Mech. B-Fluid 93 (2022) 65–92.
[27] J. Debadatta, C.B. Kishore, A numerical study of violent sloshing problems with modified MPS method, J. Hydrodyn. 29 (4) (2017) 659–667.
[28] S.C. Hwang, J.C. Park, H. Gotoh, A. Khayyer, K.J. Kang, Numerical simulations of sloshing flows with elastic baffles by using a particle-based fluid–structure interaction analysis method, Ocean Eng. 118 (2016) 227–241.
[29] Y.X. Zhang, D.C. Wan, T. Hino, Comparative study of MPS method and level-set method for sloshing flows, J. Hydrodyn. 26 (2014) 577–585.
[30] X.J. Pan, H.X. Zhang, Y.T. Lu, Numerical simulation of viscous liquid sloshing by moving-particle semi-implicit method, J. Marine. Sci. Appl. 7 (2008) 184–189.
[31] A. Khayyer, H. Gotoh, A higher order Laplacian model for enhancement and stabilization of pressure calculation by the MPS method, Appl. Ocean Res. 32 (2012) 124–131.
[32] B.H. Lee, S.M. Jeong, S.C. Hwang, J.C. Park, M.H. Kim, A particle simulation of 2D vessel motions interacting with liquid-sloshing cargo, CMES Comput. Model. Eng. Sci. 91 (1) (2013) 43–63.
[33] X. Chen, Y.L. Zhang, D.C. Wan, Numerical study of 3-D liquid sloshing in an elastic tank by MPS-FEM coupled method, J. Ship Res. 63 (3) (2019) 143–153.
[34] F.Z. Xie, W.W. Zhao, D.C. Wan, CFD simulations of three-dimensional violent sloshing flows in tanks based on MPS and GPU, J. Hydrodyn. 32 (2020) 672–683.
[35] R. Zha, H. Peng, W. Qiu, An improved higher-order moving particle semi-implicit method for simulations of two-dimensional hydroelastic slamming, Phys. Fluids 33 (2021) 037104.
[36] Y.G. Chen, W.G. Price, Numerical simulation of liquid sloshing in a partially filled container with inclusion of compressibility effects, Phys. Fluids 21 (2009) 112105.
[37] C. Lugni, M. Miozzi, M. Brocchini, O.M. Faltinsen, Evolution of the air cavity during a depressurized wave impact. I. The kinematic flow field, Phys. Fluids 22 (2010) 056101.
[38] A. Souto-Iglesias, E. Botia-Vera, A. Martín, F. Pérez-Arribas, A set of canonical problems in sloshing. Part 0: Experimental setup and data processing, Ocean Eng. 38 (2011) 1823–1830.
[39] B. Bouscasse, A. Colagrossi, A. Souto-Iglesias, J.L. Cercos-Pita, Mechanical energy dissipation induced by sloshing and wave breaking in a fully coupled angular motion system. II. Experimental investigation, Phys. Fluids 26 (2014) 033104.
[40] G. Bulian, E. Botia-Vera, A. Souto-Iglesias, Experimental sloshing pressure impacts in ensemble domain: transient and stationary statistical characteristics, Phys. Fluids 26 (2014) 032102.
[41] C. Lugni, M. Brocchini, O.M. Faltinsen, Wave impact loads: the role of the flip-through, Phys. Fluids 18 (2006) 122101.
[42] D.H. Lee, M.H. Kim, S.H. Kwon, J.W. Kim, Y.B. Lee, A parametric sensitivity study on LNG tank sloshing loads by numerical simulations, Ocean Eng. 34 (1) (2007) 3–9.
[43] Y. Shimizu, H. Gotoh, A. Khayyer, An MPS-based particle method for simulation of multiphase flows characterized by high density ratios by incorporation of space potential particle concept, Comput. Math. Appl. 76 (5) (2018) 1108–1129.
[44] Z.F. Meng, P.P. Wang, A.M. Zhang, F.R. Ming, P.N. Sun, A multiphase SPH model based on roe's approximate Riemann solver for hydraulic flows with complex interface, Comput. Methods Appl. Mech. Engrg. 318 (365) (2020) 112999.
[45] G.G. Koh, M. Gao, G. Luo, A new particle method for simulation of incompressible free surface flow problems, Internat. J. Numer. Methods Engrg. 89 (2012) 1582–1604.
[46] A. Khayyer, H. Gotoh, Enhancement of performance and stability of MPS mesh-free particle method for multiphase flows characterized by high density ratios, J. Comput. Phys. 242 (2013) 211–233.
[47] O.F. Rognebakke, J.R. Hoff, J.M. Allers, K. Berget, B.O. Bergo, R. Zhao, Experimental approaches for determining sloshing loads in LNG tanks, Trans. Soc. Naval Archit. Mar. Eng. 113 (2006) 384–401.
[48] X.F. Yang, M.B. Liu, Numerical study of Rayleigh–Taylor instability by using smoothed particle hydrodynamics, Acta Phys. Sin. 66 (2017) 164701.
[49] Z.Y. Tang, D.C. Wan, Numerical simulation of impinging jet flows by modified MPS method, Eng. Comput. 32 (4) (2015) 1153–1171.
[50] Y.L. Zhang, D.C. Wan, Numerical study of interactions between waves and free rolling body by IMPS method, Comput. Fluids 155 (2017) 124–133.
[51] Y.L. Zhang, D.C. Wan, MPS-FEM coupled method for sloshing flows in an elastic tank, Ocean Eng. 152 (2018) 416–427.
[52] Y.X. Zhang, D.C. Wan, Numerical simulation of liquid sloshing in low-filling tank by MPS, J. Hydrodyn. 27 (2012) 101–107.
[53] M. Tanaka, T. Masunaga, Stabilization and smoothing of pressure in MPS method by quasi-compressibility, J. Comput. Phys. 229 (2010) 4279–4290.
[54] S. Shao, H. Gotoh, Turbulence particle models for tracking free surfaces, J. Hydrul. Res. 43 (3) (2005) 276–289.
[55] B.H. Lee, J.C. Park, M.H. Kim, S.C. Hwang, Step-by-step improvement of MPS method in simulating violent free-surface motions and impact-loads, Comput. Methods Appl. Mech. Engrg. 200 (2011) 1113–1125.
[56] Y.X. Zhang, D.C. Wan, Apply MPS method to simulate liquid sloshing in LNG tank, in: Proceedings of the 22nd International Offshore and Polar Engineering Conference, 2012, pp. 381–391.
[57] X. Wen, W.W. Zhao, D.C. Wan, An improved moving particle semi-implicit method for interfacial flows, Appl. Ocean Res. 117 (2021) 102963.
[58] A. Shakibaeinia, Y. Jin, MPS mesh-free particle method for multiphase flow, Comput. Methods Appl. Mech. Eng. 229-232 (2012) 13–26.
[59] A. Rafiee, F. Pistani, K. Thiagarajan, Study of liquid sloshing: numerical and experimental approach, Comput. Mech. 47 (1) (2011) 6575.
[60] M. Rezavand, C. Zhang, X. Hu, A weakly compressible SPH method for violent multi-phase flows with high density ratio, J. Comput. Phys. 402 (2020) 109092.
[61] G. Duan, S. Koshizuka, B. Chen, H. Xiang, Stable multiphase moving particle semi-implicit method for incompressible interfacial flow, Comput. Methods Appl. Mech. Engrg. 318 (2017) 636–666.
[62] J.U. Brackbill, D.B. Kothe, C. Zemach, A continuum method for modeling surface tension, J. Comput. Phys. 100 (1992) 335–354.
[63] A.M. Zhang, P.N. Sun, F.R. Ming, An SPH modeling of bubble rising and coalescing in three dimensions, Comput. Methods Appl. Mech. Engrg. 294 (2015) 189–209.
[64] G. Duan, S. Koshizuka, B. Chen, A contoured continuum surface force model for particle methods, J. Comput. Phys. 298 (2015) 280–304.
[65] A. Khayyer, H. Gotoh, Modified moving particle semi-implicit methods for the prediction of 2D wave impact pressure, Coast. Eng. 56 (4) (2009) 419–440.
[66] A. Khayyer, H. Gotoh, A multiphase compressible-incompressible particle method for water slamming, Int. J. Offshore Polar 26 (1) (2016) 20–25.
[67] X.Y. Hu, N.A. Adams, A constant-density approach for incompressible multi-phase SPH, J. Comput. Phys. 228 (6) (2009) 2082–2091.
[68] X. Chen, D.C. Wan, GPU accelerated MPS method for large-scale 3-D violent free surface flows, Ocean Eng. 171 (2019) 677–694.
[69] X. Chen, D.C. Wan, Numerical simulation of three-dimensional violent free surface flows by GPU-based MPS method, Int. J. Comput. Methods 16 (4) (2019) 1–20.
[70] K. Nomura, S. Koshizuka, Y. Oka, H. Obata, Numerical analysis of droplet breakup behavior using particle method, J. Nucl. Sci. Technol. 38 (12) (2001) 1057–1064.
[71] X. Chen, X. Guang, Z.G. Sun, Improving stability of MPS method by a computational scheme based on conceptual particles, Comput. Methods Appl. Math. 278 (2014) 254–271.
[72] K. Shibata, I. Masaie, M. Kondo, K. Murotani, S. Koshizuka, Improved pressure calculation for the moving particle semi-implicit method, Comput. Part. Mech. 2 (2015) 91–108.
[73] N. Tsuruta, A. Khayyer, H. Gotoh, Space potential particles to enhance the stability of projection-based particle methods, Int. J. Comput. Fluid Dyn. 29 (2015) 100–119.